Constraint-consistent Runge–Kutta methods for one-dimensional incompressible multiphase flow

B. Sanderse [a,*], A.E.P. Veldman [b]

[a] *Centrum Wiskunde & Informatica (CWI), Amsterdam, the Netherlands*
[b] *Bernoulli Institute for Mathematics, Computer Science and Artificial Intelligence, University of Groningen, Groningen, the Netherlands*

A B S T R A C T

New time integration methods are proposed for simulating incompressible multiphase flow in pipelines described by the one-dimensional two-fluid model. The methodology is based on 'half-explicit' Runge–Kutta methods, being explicit for the mass and momentum equations and implicit for the volume constraint. These half-explicit methods are *constraint-consistent*, i.e., they satisfy the hidden constraints of the two-fluid model, namely the volumetric flow (incompressibility) constraint and the Poisson equation for the pressure. A novel analysis shows that these hidden constraints are present in the continuous, semi-discrete, and fully discrete equations.

Next to constraint-consistency, the new methods are *conservative*: the original mass and momentum equations are solved, and the proper shock conditions are satisfied; *efficient*: the implicit constraint is rewritten into a pressure Poisson equation, and the time step for the explicit part is restricted by a CFL condition based on the convective wave speeds; and *accurate*: achieving high order temporal accuracy for all solution components (masses, velocities, and pressure). High-order accuracy is obtained by constructing a new third-order Runge–Kutta method that satisfies the additional order conditions arising from the presence of the constraint in combination with time-dependent boundary conditions.

Two test cases (Kelvin–Helmholtz instabilities in a pipeline and liquid sloshing in a cylindrical tank) show that for time-independent boundary conditions the half-explicit formulation with a classic fourth-order Runge–Kutta method accurately integrates the two-fluid model equations in time while preserving all constraints. A third test case (ramp-up of gas production in a multiphase pipeline) shows that our new third-order method is preferred for cases featuring time-dependent boundary conditions.

© 2019 Elsevier Inc. All rights reserved.

1. Introduction

1.1. Background

The incompressible two-fluid model for one-dimensional multiphase flow is an important model to study, for example, the behavior of oil and gas in long pipelines. A main research area is the development of methods that accurately solve the two-fluid model in order to predict the transition from stratified flow to slug flow, and the subsequent propagation of

the generated slugs (so-called slug capturing methods). In this paper we progress towards this goal by developing efficient time integration methods for the incompressible two-fluid model in its basic form: a four-equation model (describing conservation of mass and momentum per phase), supplemented with a volume constraint (describing that the phases together exactly fill the pipeline). An important aspect in the construction of time integration methods lies in the correct treatment of this volume constraint and associated derived constraints, such as the divergence-free constraint on the mixture velocity field.

Historically, the development of efficient time integration methods for the two-fluid model hinges on the use of the pressure equation. For the *compressible* two-fluid model a hyperbolic evolution equation for the pressure can be derived by a single differentiation of the volume constraint (see e.g. [8,37]). The resulting system can be solved for example with implicit methods in order to circumvent the CFL condition associated to the acoustic waves [16,45]. However, in case the flow is incompressible, the character of the pressure equation changes from hyperbolic to elliptic, and dedicated incompressible solvers are more efficient than compressible solvers.

Different approaches to deal with this incompressible, one-dimensional, multiphase flow problem have been proposed, which will be shortly summarized here.

A first approach is to eliminate the pressure from the four-equation system and to rewrite this system into a two-equation system. This leads to the 'no-pressure wave' model or the 'fixed-flux' model suggested by [54], and used for example in [1,26,35,39]. A similar two equation model is the 'reversed density' model developed by Keyfitz et al. [31] and employed for example in [53]. In these models, the pressure is generally computed as a post-processing step. A general problem with these reduced equation systems is that they are only valid in case of smooth solutions. In the presence of shocks the wrong jump conditions are obtained [1]. Furthermore, the fixed-flux assumption often limits these studies to stationary boundary conditions.

A second approach is to keep the pressure in the formulation and to use a pressure-correction method. A pressure equation is then typically obtained by substituting the momentum equations in the combined mass conservation equation, while applying the volume constraint equation. This approach is taken by Liao et al. [33], who solve the momentum equations with an old pressure, solve for the new pressure, and then update the velocity. A slightly different approach is taken in [27,35,52], in which the pressure equation is derived from a combination of momentum and continuity equations, without using the constraint equation. A related approach is the all-speed method in the RELAP-7 code [9], based on the PCICE (pressure corrected implicit continuous-fluid eulerian) algorithm. The temporal accuracy of these approaches is mostly limited to first order, or not reported. Note that most of these methods are reminiscent of single phase incompressible (2D or 3D) Navier–Stokes solution algorithms such as SIMPLE ([41]) or PISO [28], which were developed to handle the divergence-free constraint.

The aim of this paper is to resolve the issues of these current approaches by developing high order *constraint-consistent* time integration methods for the incompressible two-fluid model equations in conservation form, including a generic (non-stationary) boundary condition treatment.

1.2. Approach and outline

In this paper we study the incompressible two-fluid model equations in conservative form. The constraint in the model has implications on all discretization aspects and we have constructed the roadmap of Fig. 1 to make this clear. First we show via a characteristic analysis that the constraint in the continuous model equations introduces two additional 'hidden' constraints (section 2, first row of Fig. 1). Second, the constraint has important consequences for the spatial discretization of the equations, in particular for the boundary conditions, which are derived in section 3. Third, in the resulting semi-discrete equations the presence of the constraint leads to a differential-algebraic equation (DAE) system that features the same two hidden constraints (section 4, second row in Fig. 1). These semi-discrete equations are discretized in time with a 'half-explicit' Runge–Kutta method and recombined into a form that highlights the hidden constraints in the equations (section 5, third row in Fig. 1). The DAE classification is used to perform the accuracy analysis, and a new third-order Runge–Kutta method will be designed such to avoid order reduction. The resulting method is a new high-order time integration method that is consistent with the constraints derived on the continuous and semi-discrete level. In summary, our novel approach follows the red dashed line in Fig. 1 and is consistent with the mantra: *discretize first, substitute next* [51].

The main advantages of this approach are that (i) the method is consistent with the constraints of the model, (ii) high-order accuracy of all solution components, including the pressure, is achieved, (iii) the original conservation equations are solved, and (iv) the approach only requires implicit treatment of the pressure equation. Furthermore, the approach has the potential to be applied to other constraint systems, such as drift-flux models and three-fluid models, and multi-dimensional applications.

2. Constraint analysis of differential equations

2.1. Governing equations incompressible flow

The incompressible two-fluid model can be derived by considering the stratified flow of liquid and gas in a pipeline (for a recent discussion of the two-fluid model, see for example [35]). For a sketch of the geometry, see Fig. 2. The main
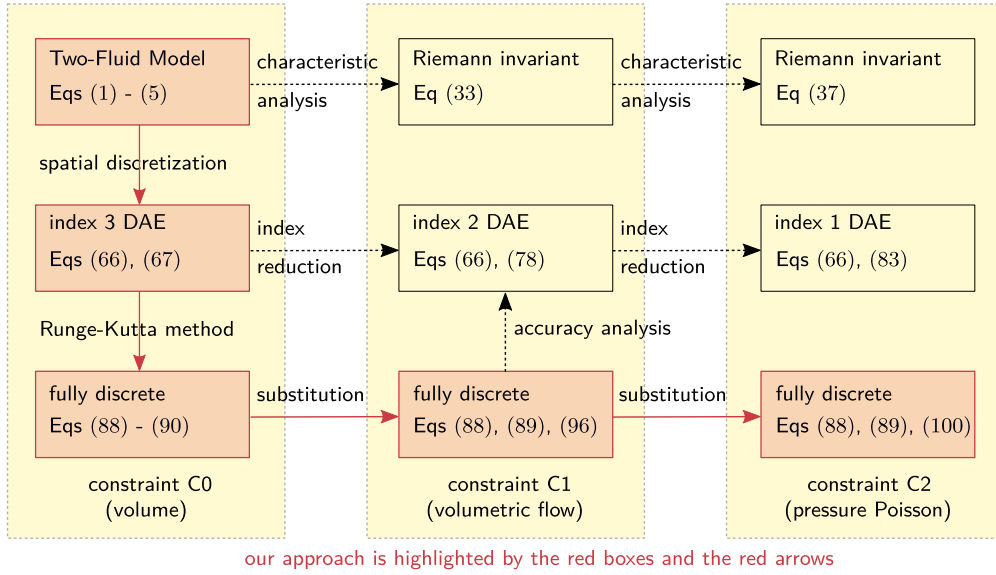
Fig. 1. Our approach to form new time integration methods for the incompressible two-fluid model follows the red boxes: *discretize first, substitute next*. (For interpretation of the colors in the figure(s), the reader is referred to the web version of this article.)
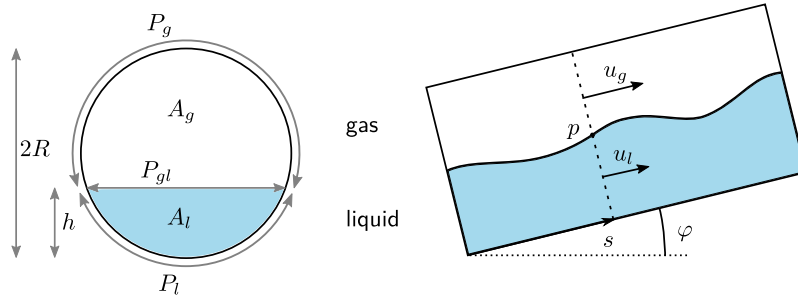

Fig. 2. Stratified flow in a pipeline. Left: cross-sectional view; right: side view.

assumptions that we make are that the flow is one-dimensional, stratified, incompressible, and isothermal. Transverse pressure variation is introduced via level gradient terms. Surface tension is neglected. This leads to the following four-equation model:

$$\frac{\partial}{\partial t}\left(\rho_g A_g\right) + \frac{\partial}{\partial s}\left(\rho_g u_g A_g\right) = 0, \tag{1}$$

$$\frac{\partial}{\partial t}\left(\rho_l A_l\right) + \frac{\partial}{\partial s}\left(\rho_l u_l A_l\right) = 0, \tag{2}$$

$$\frac{\partial}{\partial t}\left(\rho_g u_g A_g\right) + \frac{\partial}{\partial s}(\rho_g u_g^2 A_g) = -\frac{\partial p}{\partial s}A_g + E_g + \underbrace{-\tau_{gl}P_{gl} - \tau_g P_g - \rho_g A_g g_s + F_{\text{body}}A_g}_{S_g}, \tag{3}$$

$$\frac{\partial}{\partial t}\left(\rho_l u_l A_l\right) + \frac{\partial}{\partial s}(\rho_l u_l^2 A_l) = -\frac{\partial p}{\partial s}A_l + E_l + \underbrace{\tau_{gl}P_{gl} - \tau_l P_l - \rho_l A_l g_s + F_{\text{body}}A_l}_{S_l}, \tag{4}$$

supplemented with the *volume constraint equation*, which we indicate by C0:

C0: $\quad A_g + A_l = A.$ $\hspace{10cm}$ (5)

In these equations the subscript denotes either gas (g) or liquid (l). The model features four evolution equations, one constraint equation, and five unknowns (A_g, A_l, u_g, u_l, p), which are a function of the independent variables s (coordinate along the pipeline axis) and t (time). ρ denotes the density (assumed constant), A the cross-sectional area of the pipe, A_g and A_l (also referred to as the hold-ups) the cross-sectional areas occupied by the gas or liquid, u the phase velocity, p the pressure at the interface, τ the shear stress (with the wall or at the interface), g the gravitational constant, φ the

local inclination of the pipeline with respect to the horizontal, $g_n = g \cos \varphi$ and $g_s = g \sin \varphi$. The wetted and interfacial perimeters P_g, P_l and P_{gl} can be expressed in terms of the hold-ups A_g or A_l via a non-linear algebraic expression, see Appendix A.1. The same is true for the interface height h (measured from the bottom of the pipe), which appears in the expression for the level gradient terms E [45]:

$$E_g = \frac{\partial K_g}{\partial s}, \quad K_g = \rho_g g_n \left[(R - h) A_g + \frac{1}{12} P_{gl}^3 \right], \tag{6}$$

$$E_l = \frac{\partial K_l}{\partial s}, \quad K_l = \rho_l g_n \left[(R - h) A_l - \frac{1}{12} P_{gl}^3 \right]. \tag{7}$$

In these expressions R is the pipe radius. For incompressible flow these expressions simplify to $E_g = -\rho_g g_n A_g \frac{\partial h}{\partial s}$, $E_l = -\rho_l g_n A_l \frac{\partial h}{\partial s}$, but we stick to the form displayed in equation (6) because this form is conservative. The two-fluid model can also be employed for channel flow instead of pipe flow with minor modifications.

The body force F_{body} in the gas and liquid momentum equations is for example a driving pressure force for the simulations that involve periodic boundary conditions, or a source term to force an analytical solution (see Appendix B). The friction models for τ_g, τ_l and τ_{gl} are described in Appendix A.2. The source terms S_g and S_l do not contain spatial or temporal derivatives.

The two-fluid model is supplemented with initial and boundary conditions to form an initial boundary value problem. As the two-fluid model equations are conditionally hyperbolic [6,36,47], not all initial and boundary conditions guarantee that the equations remain hyperbolic. In this paper we will avoid non-hyperbolic conditions and consequently guarantee well-posedness, although we should note that for non-hyperbolic equations results have also been obtained [31].

2.2. Two-equation model

Several discretization methods for solving the two-fluid model equations (1)–(5) are based on an alternative form of the model. For the compressible model, a common approach is to expand the density in the mass conservation equations in terms of the pressure, and combine the resulting equations with the volume constraint to derive a pressure equation [8,16,17]. However, in case the fluid is incompressible, such a pressure equation becomes singular and cannot be used. A common approach is then to reduce the four-equation system to a two-equation system [1,26,39]. The basis lies in combining the mass equations and the volume constraint to derive the *volumetric flow constraint* (C1):

$$\underline{C1}: \quad \frac{\partial}{\partial s} \left(A_g u_g + A_l u_l \right) = 0. \tag{8}$$

It can be integrated in space to give, at any point in the pipeline,

$$A u_{\text{mix}} := A_g u_g + A_l u_l = V(t), \tag{9}$$

where $V(t)$ is the volumetric flow rate. The next step is to rewrite the momentum and mass equations into an equation for the difference in momenta:

$$\frac{\partial}{\partial t} \left(\rho_l u_l - \rho_g u_g \right) + \frac{\partial}{\partial s} \left(\frac{1}{2} \left(\rho_l u_l^2 - \rho_g u_g^2 \right) \right) = -(\rho_l - \rho_g) g_n \frac{\partial h}{\partial s} + \frac{S_l}{A_l} - \frac{S_g}{A_g}. \tag{10}$$

At the same time, the mass equations can be combined to give

$$\frac{\partial}{\partial t} \left(\rho_g A_g + \rho_l A_l \right) + \frac{\partial}{\partial s} \left(\rho_g u_g A_g + \rho_l u_l A_l \right) = 0. \tag{11}$$

The 'conservative' (pressure-free) combined momentum equation (10) and the conservative combined mass equation (11) form a two-equation system, which can be numerically solved when supplemented with the volume constraint (5) and volumetric flow constraint (9). However, this reduced pressure-free model is only equivalent to the original two-fluid model for sufficiently smooth solutions. In case shock waves appear in the solution, the pressure-free model is not equivalent, and will generally exhibit different weak solutions [2,32]. An example of shock waves in the two-fluid model are roll waves [54], for which it has been shown that the conservative and non-conservative equation systems indeed lead to different solutions [2,44]. Consequently, we will *not* pursue the two-equation system as a starting point for the development of time integration methods, but instead use the original conservation equations (1)–(4).[1]

---

[1] We note that the momentum equations in the four-equation model are not fully conservative due to the presence of the hold-up fractions in the pressure gradient terms. This is a topic of study in itself, and we refer the interested reader to [13,50].

2.3. Constraint equations from characteristic analysis

The governing equations of the two-fluid model describe the change in mass and momentum of each phase, commonly expressed by the vector of conservative variables

$$
\boldsymbol{U} = \begin{pmatrix} \rho_g A_g \\ \rho_l A_l \\ \rho_g u_g A_g \\ \rho_l u_l A_l \end{pmatrix}.
\tag{12}
$$

As mentioned, the equations cannot be written in full conservative form, but fortunately they can be written in quasi-linear form in terms of the primitive variables $\boldsymbol{W}$,

$$
\boldsymbol{A}(\boldsymbol{W}) \frac{\partial \boldsymbol{W}}{\partial t} + \boldsymbol{B}(\boldsymbol{W}) \frac{\partial \boldsymbol{W}}{\partial s} + \boldsymbol{S}(\boldsymbol{W}) = \boldsymbol{0},
\tag{13}
$$

where we choose $\boldsymbol{W} = (A_l, u_l, u_g, p)^T$. The dependence of $\boldsymbol{A}$, $\boldsymbol{B}$ and $\boldsymbol{S}$ on $\boldsymbol{W}$ will not be explicitly indicated in the sequel. The matrices $\boldsymbol{A}$ and $\boldsymbol{B}$ and source term $\boldsymbol{S}$ can be simplified, by multiplying the mass equations by their respective velocities and adding them to the momentum equations, and by dividing by the respective cross-sectional areas:

$$
\boldsymbol{A} = \begin{pmatrix} 1 & 0 & 0 & 0 \\ -1 & 0 & 0 & 0 \\ 0 & \rho_l & 0 & 0 \\ 0 & 0 & \rho_g & 0 \end{pmatrix}, \qquad
\boldsymbol{B} = \begin{pmatrix} u_l & A_l & 0 & 0 \\ -u_g & 0 & A_g & 0 \\ -\frac{1}{A_l}\frac{\partial K_l}{\partial A_l} & \rho_l u_l & 0 & 1 \\ +\frac{1}{A_g}\frac{\partial K_g}{\partial A_g} & 0 & \rho_g u_g & 1 \end{pmatrix}, \qquad
\boldsymbol{S} = \begin{pmatrix} 0 \\ 0 \\ -S_l/A_l \\ -S_g/A_g \end{pmatrix}.
\tag{14}
$$

In this derivation the constraint has been substituted, in the form $\frac{\partial A_g}{\partial t} = -\frac{\partial A_l}{\partial t}$ and $\frac{\partial A_g}{\partial s} = -\frac{\partial A_l}{\partial s}$. The derivatives of the level gradient terms read

$$
\frac{\partial K_l}{\partial A_l} = -\rho_l g_n H_l, \qquad \frac{\partial K_g}{\partial A_g} = \rho_g g_n H_g,
\tag{15}
$$

where $H_l/A_l = H_g/A_g = \frac{\partial h}{\partial A_l}$ (similar to the derivation in [6]).

The eigenvalues are found from the generalized eigenvalue problem

$$
\det(\boldsymbol{B} - \lambda \boldsymbol{A}) = 0.
\tag{16}
$$

Since $\boldsymbol{A}$ is rank-deficient (rank($\boldsymbol{A}$) = 3), the number of eigenvalues is lower than the dimension of the matrix [18]. Two of the roots are given by

$$
\lambda_{1,2} = \frac{(\rho u)^* \pm \xi}{\rho^*},
\tag{17}
$$

where, in the notation from Akselsen [2], we define the averaging operator $(.)^*$ as:

$$
(.)^* := \frac{(.)_l}{A_l} + \frac{(.)_g}{A_g},
\tag{18}
$$

and furthermore

$$
\xi = \sqrt{ \rho^*(\rho_l - \rho_g) g_n \frac{\partial h}{\partial A_l} - \frac{\rho_g \rho_l}{A_g A_l}(u_g - u_l)^2 }.
\tag{19}
$$

The characteristic polynomial corresponding to the eigenvalue problem is given by:

$$
\rho_l A_g (u_l - \lambda)^2 + \rho_g A_l (u_g - \lambda)^2 + (\rho_l - \rho_g) A_g A_l g_n \frac{\partial h}{\partial A_l} = 0,
\tag{20}
$$

and the two eigenvalues $\lambda_{1,2}$ are real provided that:

$$
(u_g - u_l)^2 \le \frac{\rho_l - \rho_g}{\rho^*} g_n \frac{\partial h}{\partial A_l},
\tag{21}
$$

which is known as the inviscid Kelvin–Helmholtz limit. The (left) eigenvectors related to $\lambda_{1,2}$ are found as follows

$$\boldsymbol{l}_1 = \left(-\frac{\rho_l}{A_l} \frac{\frac{\rho_g}{A_g}(u_g - u_l) - \xi}{\rho^*} \quad -\frac{\rho_g}{A_g} \frac{\frac{\rho_l}{A_l}(u_g - u_l) + \xi}{\rho^*} \quad -1 \quad 1 \right), \tag{22}$$

$$\boldsymbol{l}_2 = \left(-\frac{\rho_l}{A_l} \frac{\frac{\rho_g}{A_g}(u_g - u_l) + \xi}{\rho^*} \quad -\frac{\rho_g}{A_g} \frac{\frac{\rho_l}{A_l}(u_g - u_l) - \xi}{\rho^*} \quad -1 \quad 1 \right). \tag{23}$$

The Riemann invariant related to each eigenvector follows by multiplying the original PDEs with the eigenvector. For λ_1 and $\boldsymbol{l}_1$ this yields

$$\boldsymbol{l}_1 \cdot \left(\boldsymbol{A} \frac{\partial \boldsymbol{W}}{\partial t} + \boldsymbol{B} \frac{\partial \boldsymbol{W}}{\partial s} + \boldsymbol{S} \right) = 0, \tag{24}$$

giving the Riemann invariant

$$\xi \frac{\partial A_l}{\partial t} - \rho_l \frac{\partial u_l}{\partial t} + \rho_g \frac{\partial u_g}{\partial t} + \lambda_1 \xi \frac{\partial A_l}{\partial s} - \lambda_1 \rho_l \frac{\partial u_l}{\partial s} + \lambda_1 \rho_g \frac{\partial u_g}{\partial s} + \frac{S_l}{A_l} - \frac{S_g}{A_g} = 0, \tag{25}$$

which can be written as

$$\xi \frac{\mathrm{d} A_l}{\mathrm{d} t} - \rho_l \frac{\mathrm{d} u_l}{\mathrm{d} t} + \rho_g \frac{\mathrm{d} u_g}{\mathrm{d} t} = \frac{S_g}{A_g} - \frac{S_l}{A_l}, \tag{26}$$

with $\frac{\mathrm{d}}{\mathrm{d}t} = \frac{\partial}{\partial t} + \lambda_1 \frac{\partial}{\partial s}$. For the second eigenvalue and eigenvector $\lambda_2, \boldsymbol{l}_2$ we similarly get

$$-\xi \frac{\mathrm{d} A_l}{\mathrm{d} t} - \rho_l \frac{\mathrm{d} u_l}{\mathrm{d} t} + \rho_g \frac{\mathrm{d} u_g}{\mathrm{d} t} = \frac{S_g}{A_g} - \frac{S_l}{A_l}, \tag{27}$$

with $\frac{\mathrm{d}}{\mathrm{d}t} = \frac{\partial}{\partial t} + \lambda_2 \frac{\partial}{\partial s}$. These eigenvalues and Riemann invariants are similar to the ones typically obtained for the two-equation system mentioned in section 2.2, see [1,22,42], and will be used for our characteristic boundary condition treatment in section 3.2. These two eigenvalues and Riemann invariants reflect the hyperbolic character of the two-fluid model, but the effect of the third and fourth eigenvalue has been lost, and in particular the elliptic behavior of the pressure is missing.

Here we extend the characteristic analysis to include the third and fourth eigenvalue of the system. This requires the consideration of the *inverse* eigenvalue problem, $\boldsymbol{A}\boldsymbol{v} = \mu \boldsymbol{B}\boldsymbol{v}$, with the determinant equation

$$\det(\mu \boldsymbol{B} - \boldsymbol{A}) = 0, \tag{28}$$

leading to the following characteristic polynomial

$$\mu^2 \left(\rho_l A_g (\mu u_l - 1)^2 + \rho_g A_l (\mu u_g - 1)^2 \right) + \mu^2 (\rho_l - \rho_g) A_g A_l g_n \frac{\partial h}{\partial A_l} = 0. \tag{29}$$

This equation has solutions $\mu_{1,2} = 1/\lambda_{1,2}$, and $\mu_{3,4} = 0$, indicating that $\lambda_{3,4}$ are infinite (see also Drew and Passman [15]). The left eigenvector of the inverse eigenvector problem is the same as of the original eigenvector problem, and for $\mu_3 = 0$ the condition $\boldsymbol{l}_3 \cdot \boldsymbol{A} = 0$ leads to:

$$\boldsymbol{l}_3 = \begin{pmatrix} 1 & 1 & 0 & 0 \end{pmatrix}. \tag{30}$$

The corresponding 'Riemann invariant' follows as:

$$\boldsymbol{l}_3 \cdot \left(\boldsymbol{A} \frac{\partial \boldsymbol{W}}{\partial t} + \boldsymbol{B} \frac{\partial \boldsymbol{W}}{\partial s} + \boldsymbol{S} \right) = 0, \tag{31}$$

leading to

$$(u_l - u_g) \frac{\partial A_l}{\partial s} + A_l \frac{\partial u_l}{\partial s} + A_g \frac{\partial u_g}{\partial s} = 0, \tag{32}$$

or equivalently

$$\underline{\text{C1}}: \qquad \frac{\partial}{\partial s} \left(u_l A_l + u_g A_g \right) = 0. \tag{33}$$

Thus, this means that: *the third 'Riemann invariant' corresponds to the volumetric flow constraint* (8).

To find an eigenvector associated with the fourth eigenvalue $\mu_4 = 0$, we resort to a generalized eigenvector via the application of Jordan theory:

$$\boldsymbol{l}_4 \cdot (\boldsymbol{A} - \mu_4 \boldsymbol{B}) = \boldsymbol{l}_3 \cdot \boldsymbol{B} = \begin{pmatrix} u_l - u_g & A_l & A_g & 0 \end{pmatrix}, \tag{34}$$

which leads to ($\mu_4 = 0$)

$$\boldsymbol{l}_4 = \begin{pmatrix} u_l & u_g & A_l/\rho_l & A_g/\rho_g \end{pmatrix}. \tag{35}$$

Carrying out again the multiplication with the original PDE leads to

$$\frac{\partial}{\partial t}(u_l A_l + u_g A_g) + \frac{\partial}{\partial s}(u_l^2 A_l + u_g^2 A_g) = -\left(\frac{A_l}{\rho_l} + \frac{A_g}{\rho_g}\right)\frac{\partial p}{\partial s} + \frac{E_g}{\rho_g} + \frac{E_l}{\rho_l} + \frac{S_g}{\rho_g} + \frac{S_l}{\rho_l}. \tag{36}$$

This is a combination of the momentum equations (after division by the respective densities) which involves the time derivative of the total volumetric flow $V(t)$ (see (9)):

$$\left(\frac{A_l}{\rho_l} + \frac{A_g}{\rho_g}\right)\frac{\partial p}{\partial s} = -\frac{\mathrm{d}V(t)}{\mathrm{d}t} - \frac{\partial}{\partial s}(u_l^2 A_l + u_g^2 A_g) + \frac{E_g}{\rho_g} + \frac{E_l}{\rho_l} + \frac{S_g}{\rho_g} + \frac{S_l}{\rho_l}. \tag{37}$$

Further differentiation with respect to s gives the following pressure constraint:

$$\underline{\text{C2}}: \quad \frac{\partial}{\partial s}\left(\left(\frac{A_g}{\rho_g} + \frac{A_l}{\rho_l}\right)\frac{\partial p}{\partial s}\right) = -\frac{\partial^2}{\partial s^2}(u_g^2 A_g + u_l^2 A_l) + \frac{\partial}{\partial s}\left(\frac{E_g}{\rho_g} + \frac{E_l}{\rho_l}\right) + \frac{\partial}{\partial s}\left(\frac{S_g}{\rho_g} + \frac{S_l}{\rho_l}\right). \tag{38}$$

The fourth 'Riemann invariant' corresponds to a Poisson-type equation for the pressure. Effectively, this equation is obtained by taking the time derivative of the mixture equation (33), and by substituting the spatially-differentiated momentum equations. It hinges on the fact that *the time derivative of the spatial terms in the mass equations is equal to the spatial derivative of the temporal terms in the momentum equations.* This is an important observation that will be used in constructing a discrete approximation and a consistent discrete pressure equation. Equations (33) and (38) are two hidden constraints of the continuous model equations and can be used for constructing an efficient numerical solution algorithm.

Strictly speaking, the full two-fluid model is parabolic, because it has real eigenvalues with a degenerate set of eigenvectors. Practically speaking, the system of equations has a hyperbolic part, with two real eigenvalues, and an elliptic part, corresponding to the Poisson-like equation for the pressure. The pressure is a Lagrange multiplier that makes the mixture velocity field divergence free.

To conclude, the first novel result of this paper is that *the two 'Riemann invariants' associated with the infinite eigenvalues are the hidden constraints of the system. They are satisfied instantaneously, at each moment in time.* This means, for example, that no explicit initial condition for the pressure is required, since it follows from the initial condition for the phase velocities and hold-up fractions. Furthermore, the presence of infinite eigenvalues requires an (at least partially) implicit time integration strategy.

The insights obtained from the characteristic analysis in this section will be employed in the next sections to construct a new boundary condition treatment and to interpret our new time integration strategy.

3. Spatial discretization and boundary conditions

3.1. Discretization at interior points

The spatial discretization is on a staggered grid, consisting of N 'pressure' and $N+1$ 'velocity' volumes. The midpoints of the velocity volumes lie on the faces of the pressure volumes. The pressure, density, hold-up and mass are defined in the center of the pressure volumes, whereas the velocity and momentum are defined in the center of the velocity volumes, see Fig. 3. For details we refer to [45]. The unknowns are the vector of conservative variables $U(t)$:

$$U(t) = \begin{pmatrix} m_g \\ m_l \\ I_g \\ I_l \end{pmatrix} = \begin{pmatrix} [(\rho_g A_g)_1 \dots (\rho_g A_g)_N]^T \\ [(\rho_l A_l)_1 \dots (\rho_l A_l)_N]^T \\ [(\rho_g A_g u_g)_{1/2} \dots (\rho_g A_g u_g)_{N+1/2}]^T \\ [(\rho_l A_l u_l)_{1/2} \dots (\rho_l A_l u_l)_{N+1/2}]^T \end{pmatrix}, \tag{39}$$

and the pressure:

$$p(t) = [p_1 \dots p_N]^T. \tag{40}$$

Note that m_g, m_l, I_g and I_l are vectors, containing mass and momentum (per unit pipe length) at the pressure and velocity volumes, respectively. $U(t)$ and $p(t)$ are both a function of time only.

We start with conservation of mass for phase β (β is liquid or gas). Integration of equation (2) in s-direction over a pressure volume gives:

$$\frac{\mathrm{d}}{\mathrm{d}t}\left(m_{\beta,i}\Delta s_i\right) + I_{\beta,i+1/2} - I_{\beta,i-1/2} = 0, \tag{41}$$
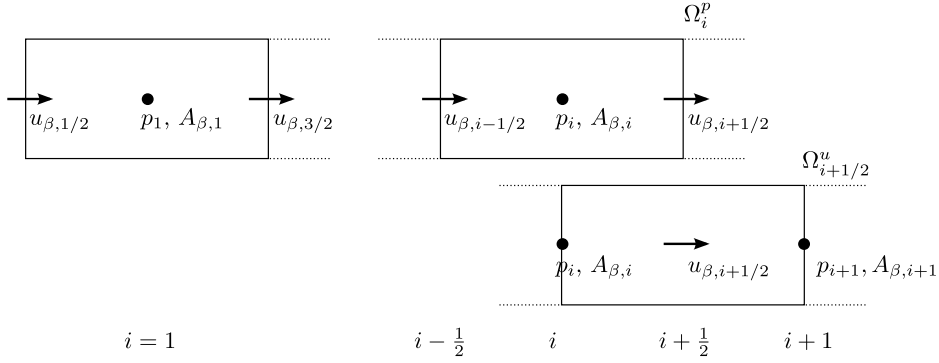
Fig. 3. Staggered grid layout including left boundary.

where the convective fluxes can be directly expressed in terms of the momenta I at the staggered locations, so no approximation is involved in this term.

For conservation of momentum we proceed in a similar way. Integration of (4) in s-direction over a velocity volume gives:

$$\frac{\mathrm{d}}{\mathrm{d}t}\left(I_{\beta,i+1/2}\Delta s_{i+1/2}\right) + \left(\rho_\beta A_\beta\right)_{i+1}\left(u_{\beta,i+1}\right)^2 - \left(\rho_\beta A_\beta\right)_i\left(u_{\beta,i}\right)^2$$
$$= -A_{\beta,i+1/2}\left(p_{i+1} - p_i\right) + E_{\beta,i+1/2} + S_{\beta,i+1/2}\Delta s_{i+1/2}, \tag{42}$$

and the level gradient terms for the gas and liquid are given by ($+$ for gas, $-$ for liquid)

$$E_{\beta,i+1/2} = \rho_\beta g_n\left(\left(hA_\beta \pm \frac{1}{12}P_{gl}^3\right)_{i+1} - \left(hA_\beta \pm \frac{1}{12}P_{gl}^3\right)_i\right). \tag{43}$$

The convective term in the momentum equation requires approximation; in the test cases in this work we have simply used a central approximation, $u_{\beta,i} = \frac{1}{2}(u_{\beta,i+1/2} + u_{\beta,i-1/2})$.

The system is closed with the volume constraint (5), which is written in terms of the phase masses m_β as:

$$\frac{m_g}{\rho_g} + \frac{m_l}{\rho_l} - A = 0. \tag{44}$$

We stress that the unsteady term in the momentum equation and the mass fluxes in the mass equations both contain the same quantity $I_\beta = \rho_\beta A_\beta u_\beta$. This ensures a discrete coupling between the mass and momentum equations in the same way as in the continuous case, where the incompressible pressure equation was derived by equating the time differentiation of the flux terms in the mass equations to the spatial differentiation of the unsteady terms in the momentum equations. This coupling is naturally achieved by the use of a staggered grid.

3.2. Boundary conditions

The boundary conditions should be consistent with the characteristic directions (17) and eigenvectors (22)–(23). We rewrite the Riemann invariants, similar to (24), in matrix notation as

$$\boldsymbol{LA}\frac{\partial \boldsymbol{W}}{\partial t} + \boldsymbol{LB}\frac{\partial \boldsymbol{W}}{\partial t} + \boldsymbol{LS} = 0, \tag{45}$$

where $\boldsymbol{L}$ is the matrix that contains the left eigenvectors $\boldsymbol{l}_i$ as rows. Written in full, this gives

$$\begin{pmatrix} \xi & -\rho_l & \rho_g & 0 \\ -\xi & -\rho_l & \rho_g & 0 \\ 0 & 0 & 0 & 0 \\ u_l - u_g & A_l & A_g & 0 \end{pmatrix}\begin{pmatrix} \frac{\partial A_l}{\partial t} \\ \frac{\partial u_l}{\partial t} \\ \frac{\partial u_g}{\partial t} \\ \frac{\partial p}{\partial t} \end{pmatrix} + \begin{pmatrix} \lambda_1\xi & -\lambda_1\rho_l & \lambda_1\rho_g & 0 \\ -\lambda_2\xi & -\lambda_2\rho_l & \lambda_2\rho_g & 0 \\ u_l - u_g & A_l & A_g & 0 \\ u_l^2 - u_g^2 + \tilde{K} & 2u_l A_l & 2u_g A_g & \frac{A_g}{\rho_g} + \frac{A_l}{\rho_l} \end{pmatrix}\begin{pmatrix} \frac{\partial A_l}{\partial s} \\ \frac{\partial u_l}{\partial s} \\ \frac{\partial u_g}{\partial s} \\ \frac{\partial p}{\partial s} \end{pmatrix} + \begin{pmatrix} \frac{S_l}{A_l} - \frac{S_g}{A_g} \\ \frac{S_l}{A_l} - \frac{S_g}{A_g} \\ 0 \\ -\frac{S_g}{\rho_g} - \frac{S_l}{\rho_l} \end{pmatrix} = 0, \tag{46}$$

where $\tilde{K} = -\frac{1}{\rho_l}\frac{\partial K_l}{\partial A_l} + \frac{1}{\rho_g}\frac{\partial K_g}{\partial A_g}$.

In classic hyperbolic systems, boundary conditions are prescribed corresponding to the number of incoming waves and the equations for the evolution of the remaining components follows from the characteristic equations, see e.g. [48]. For
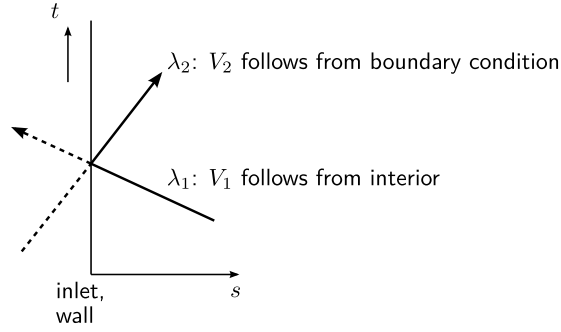
Fig. 4. Characteristics at the left boundary, used for the inflow and solid wall boundary condition.

the compressible two-fluid model such an approach has been outlined in Olsen [38], using an explicit time integration method. For the incompressible two-fluid model, the mixed hyperbolic-elliptic character of the equations requires an (at least partially) implicit approach, which we propose next.

We make the following observations based on (46). First, the two characteristic (hyperbolic) equations link changes in the hold-up A_l to changes in the phase velocities u_l, u_g, independent of the pressure. Second, there is no evolution equation for the pressure, but only an equation for its spatial derivative (fourth row), which can be interpreted as a boundary condition for the pressure. This suggests the following strategy: update the hold-up and phase velocities according to a characteristic treatment (rows $1 + 2$), and then solve a pressure equation with an (implied) boundary condition for the pressure (row 4), such that the mixture velocity field is divergence free (row 3).

3.2.1. Inflow conditions and solid wall conditions

At a pipe inlet, it is common that the liquid and gas mass flows are given as a function of time:

$$I_g(s = 0, t) = \rho_g A_g u_g = I_{g,\text{inlet}}(t), \qquad I_l(s = 0, t) = \rho_l A_l u_l = I_{l,\text{inlet}}(t). \tag{47}$$

We will assume that not only the actual mass flows are available, but also the time derivatives $\dot{I}_{g,\text{inlet}}$ and $\dot{I}_{l,\text{inlet}}$. Solid walls are a special case for which we impose the conditions

$$u_g = u_l = 0, \qquad \frac{\partial u_g}{\partial t} = \frac{\partial u_l}{\partial t} = 0. \tag{48}$$

The challenge is to find an evolution equation for the hold-up A_l at the boundary that is consistent with the characteristic equations.

Consider a boundary at $s = 0$, as shown in Fig. 4, and assume an incoming wave $\lambda_2 > 0$ and an outgoing wave $\lambda_1 < 0$. The characteristic equations are

$$\begin{pmatrix} \xi & -\rho_l & \rho_g \\ -\xi & -\rho_l & \rho_g \end{pmatrix} \begin{pmatrix} \frac{\partial A_l}{\partial t} \\ \frac{\partial u_l}{\partial t} \\ \frac{\partial u_g}{\partial t} \end{pmatrix} + \begin{pmatrix} \lambda_1 \xi & -\lambda_1 \rho_l & \lambda_1 \rho_g \\ -\lambda_2 \xi & -\lambda_2 \rho_l & \lambda_2 \rho_g \end{pmatrix} \begin{pmatrix} \frac{\partial A_l}{\partial s} \\ \frac{\partial u_l}{\partial s} \\ \frac{\partial u_g}{\partial s} \end{pmatrix} + \begin{pmatrix} \frac{S_l}{A_l} - \frac{S_g}{A_g} \\ \frac{S_l}{A_l} - \frac{S_g}{A_g} \end{pmatrix} = 0, \tag{49}$$

or

$$\begin{pmatrix} \xi & -\rho_l & \rho_g \\ -\xi & -\rho_l & \rho_g \end{pmatrix} \begin{pmatrix} \frac{\partial A_l}{\partial t} \\ \frac{\partial u_l}{\partial t} \\ \frac{\partial u_g}{\partial t} \end{pmatrix} + \begin{pmatrix} \lambda_1 V_1 \\ \lambda_2 V_2 \end{pmatrix} + \begin{pmatrix} \frac{S_l}{A_l} - \frac{S_g}{A_g} \\ \frac{S_l}{A_l} - \frac{S_g}{A_g} \end{pmatrix} = 0, \tag{50}$$

where

$$\begin{pmatrix} V_1 \\ V_2 \end{pmatrix} = \begin{pmatrix} \xi & -\rho_l & \rho_g \\ -\xi & -\rho_l & \rho_g \end{pmatrix} \begin{pmatrix} \frac{\partial A_l}{\partial s} \\ \frac{\partial u_l}{\partial s} \\ \frac{\partial u_g}{\partial s} \end{pmatrix}. \tag{51}$$

The characteristic equations feature time derivatives of the velocity; in order to obtain expressions in terms of mass flows we expand the mass flows in terms of velocity and hold-up changes as follows:

$$\frac{\partial I_g}{\partial t} = \rho_g A_g \frac{\partial u_g}{\partial t} + \rho_g u_g \frac{\partial A_g}{\partial t}. \tag{52}$$

We can rewrite this equation into

$$\rho_g \frac{\partial u_g}{\partial t} = \frac{\frac{\partial I_g}{\partial t} + \rho_g u_g \frac{\partial A_l}{\partial t}}{A_g}, \tag{53}$$

and similarly

$$\rho_l \frac{\partial u_l}{\partial t} = \frac{\frac{\partial I_l}{\partial t} - \rho_l u_l \frac{\partial A_l}{\partial t}}{A_l}. \tag{54}$$

Substituting these expressions into the characteristic equations (50) yields

$$\begin{pmatrix} \xi + \frac{\rho_g u_g}{A_g} + \frac{\rho_l u_l}{A_l} & \frac{-1}{A_l} & \frac{1}{A_g} \\ -\xi + \frac{\rho_g u_g}{A_g} + \frac{\rho_l u_l}{A_l} & \frac{-1}{A_l} & \frac{1}{A_g} \end{pmatrix} \begin{pmatrix} \frac{\partial A_l}{\partial t} \\ \frac{\partial I_l}{\partial t} \\ \frac{\partial I_g}{\partial t} \end{pmatrix} + \begin{pmatrix} \lambda_1 V_1 \\ \lambda_2 V_2 \end{pmatrix} + \begin{pmatrix} \frac{S_l}{A_l} - \frac{S_g}{A_g} \\ \frac{S_l}{A_l} - \frac{S_g}{A_g} \end{pmatrix} = 0. \tag{55}$$

Since λ_1 corresponds to the wave that carries information from the interior to the boundary, V_1 is known from the solution in the interior of the domain. To obtain an equation for V_2 that uses the given boundary conditions for $\frac{\partial I_g}{\partial t}$ and $\frac{\partial I_l}{\partial t}$, we add the two characteristic equations in such a way that the hold-up term disappears:

$$2\xi \begin{pmatrix} \frac{-1}{A_l} & \frac{1}{A_g} \end{pmatrix} \begin{pmatrix} \frac{\partial I_l}{\partial t} \\ \frac{\partial I_g}{\partial t} \end{pmatrix} + (\xi - k)\lambda_1 V_1 + (\xi + k)\lambda_2 V_2 + 2\xi \left(\frac{S_l}{A_l} - \frac{S_g}{A_g} \right) = 0, \tag{56}$$

where

$$k = (\rho u)^* = \frac{\rho_g u_g}{A_g} + \frac{\rho_l u_l}{A_l}, \tag{57}$$

and $\lambda_2 V_2$ follows as

$$\lambda_2 V_2 = -\frac{1}{\xi + k} \left[(\xi - k)\lambda_1 V_1 + 2\xi \begin{pmatrix} \frac{-1}{A_l} & \frac{1}{A_g} \end{pmatrix} \begin{pmatrix} \frac{\partial I_l}{\partial t} \\ \frac{\partial I_g}{\partial t} \end{pmatrix} + 2\xi \left(\frac{S_l}{A_l} - \frac{S_g}{A_g} \right) \right]. \tag{58}$$

The solid wall boundary condition is a special case of this equation obtained when setting $k = 0$ and $\frac{\partial I_l}{\partial t} = \frac{\partial I_g}{\partial t} = 0$. The boundary condition for $\frac{\partial A_l}{\partial t}$ follows from subtracting the two characteristic equations, which gives

$$\left(\frac{\partial A_l}{\partial t} \right)_{\text{inlet}} = \frac{\lambda_2 V_2 - \lambda_1 V_1}{2\xi}, \tag{59}$$

and substituting equation (58) for $\lambda_2 V_2$. The treatment of an inflow or solid boundary at the right side of the domain $(s = L)$ follows in a similar manner.

Given the time derivative of the liquid hold-up fraction, equation (59), we now have a complete description for the evolution of the conservative variables U at the boundary:

$$\frac{\mathrm{d} m_{g,1/2}}{\mathrm{d} t} = -\rho_g \left(\frac{\partial A_l}{\partial t} \right)_{\text{inlet}}, \tag{60}$$

$$\frac{\mathrm{d} m_{l,1/2}}{\mathrm{d} t} = \rho_l \left(\frac{\partial A_l}{\partial t} \right)_{\text{inlet}}, \tag{61}$$

$$I_{g,1/2} = I_{g,\text{inlet}}, \tag{62}$$

$$I_{l,1/2} = I_{l,\text{inlet}}. \tag{63}$$

The prescription of I_g and I_l in this way will be denoted as boundary conditions in *strong form*. The disadvantage of the strong form is that order reduction can appear in the time integration method, as will become clear in section 5.2. An alternative is to specify the boundary conditions in *weak form* via the time derivatives, and to integrate these values in time:

$$\frac{\mathrm{d} I_{g,1/2}}{\mathrm{d} t} = \dot{I}_{g,\text{inlet}}, \tag{64}$$

$$\frac{\mathrm{d} I_{l,1/2}}{\mathrm{d} t} = \dot{I}_{l,\text{inlet}}. \tag{65}$$

However, this introduces a time integration error at the boundary points. Our preferred approach is the strong form, i.e. assume that $I_{g,\text{inlet}}(t)$ and $I_{l,\text{inlet}}(t)$ are known, obtain the time derivatives for evaluating (58) by analytical or numerical differentiation, and then apply a custom-made Runge–Kutta method that prevents order reduction.
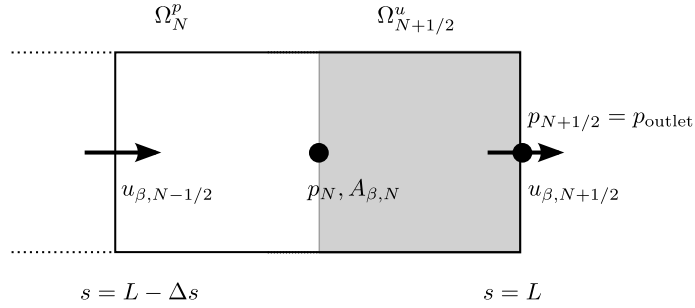
Fig. 5. Velocity volume (shaded) at an outflow boundary.

The pressure on the boundary, $p_{1/2}$, is obtained by linear extrapolation of the pressure at the first two interior points, and its value does not influence the solution of U at the interior points. The pressure at the interior points, $p_1, \ldots p_N$, is determined by the pressure Poisson equation. As will be detailed when discussing the time integration method, the pressure Poisson equation is such that the velocity field becomes divergence-free (C1), which in turn makes that the volume constraint is satisfied (C0). Similar to the case of the (single-phase, 2D or 3D) incompressible Navier–Stokes equations [20, 51], also in this 1D incompressible two-fluid model *no boundary condition for the pressure* needs to be prescribed. The pressure boundary conditions are *implied* by the discretization of the constraint equation, and are a consistent approximation to $\frac{\partial p}{\partial s}$ as given by the last equation in (46). Only in the case of an outflow boundary, at which a pressure value is prescribed, a pressure boundary condition is necessary. This is detailed next.

3.2.2. Outflow conditions

At outflow boundaries a similar approach is taken as is common for the (single-phase) incompressible Navier–Stokes equations [46]. We consider a 'half' finite volume for the momentum equations, as shown in Fig. 5. In this volume we solve the momentum equations in the same way as in the interior points, with the only difference that the pressure is specified in the boundary point: $p_{N+1/2} = p_{\text{outlet}}$. The momentum equations yield expressions for the time derivatives of $I_{g,N+1/2}$ and $I_{l,N+1/2}$, which are subsequently used together with the characteristic treatment outlined before to obtain an equation for the hold-ups, viz. (59).

3.3. Summary

In this section the characteristic directions and corresponding Riemann invariants derived in section 2 have been used to derive the second novel contribution of this paper: a new boundary condition treatment. The treatment is not only consistent with the wave directions but also with the constraints through the use of the pressure equation. No boundary conditions need to be prescribed for this pressure equation, which is consistent with the continuous model formulation for which no pressure boundary conditions were specified either.

4. Constraint analysis of differential algebraic equations

In this section we treat the constraint analysis of the semi-discrete equations as indicated in the second row in Fig. 1.

4.1. DAE formulation

The semi-discrete equations (41)–(42) supplemented with boundary conditions (60)–(61) can be rewritten in terms of the differential unknowns $U(t) = [m(t), I(t)]^T$ and algebraic unknowns $p(t)$ as a semi-explicit differential-algebraic equation (DAE) system:

$$\dot{U}(t) := \frac{\mathrm{d}U(t)}{\mathrm{d}t} = F(U(t), p(t), t), \tag{66}$$

$$\underline{\text{C0}}: \quad g(U(t)) = 0, \tag{67}$$

where

$$F(U(t), p(t)) := \begin{bmatrix} F_m(I(t), t) \\ F_I(m(t), I(t), t) - H(m(t))p(t) \end{bmatrix}, \tag{68}$$

and

$$F_m(I(t), t) := -DI(t) - b(t), \tag{69}$$

$$g(U(t)) := Q m(t) - A. \tag{70}$$

It is important to note that – in contrast to the compressible two-fluid model – the constraint equation does not depend on the pressure. This has important consequences for the index of the DAE system.

We have defined the following variables:

$$m(t) = \begin{bmatrix} m_g(t) \\ m_l(t) \end{bmatrix}, \qquad I(t) = \begin{bmatrix} I_g(t) \\ I_l(t) \end{bmatrix}, \qquad b(t) = \begin{bmatrix} b_g(t) \\ b_l(t) \end{bmatrix}, \tag{71}$$

and the matrices

$$H(m(t)) = \begin{bmatrix} Rm_g(t) \\ Rm_l(t) \end{bmatrix} G, \qquad Q = \begin{bmatrix} \mathbb{I}/\rho_g & \mathbb{I}/\rho_l \end{bmatrix}, \qquad D = \begin{bmatrix} D_p & 0 \\ 0 & D_p \end{bmatrix}. \tag{72}$$

$\mathbb{I}$ is the $N \times N$ identity matrix, and D_p and G are differencing operators that compute differences from volume faces to midpoints or vice versa. For example, with periodic boundary conditions we have the $N \times N$ matrices

$$D_p = \begin{pmatrix} -1 & 1 & & \\ & \ddots & \ddots & \\ & & -1 & 1 \\ 1 & & & -1 \end{pmatrix}, \qquad G = \begin{pmatrix} 1 & & & -1 \\ -1 & 1 & & \\ & \ddots & \ddots & \\ & & -1 & 1 \end{pmatrix}. \tag{73}$$

R is an interpolation matrix that computes averages on cell interfaces based on cell midpoint values. b_β contains boundary conditions, e.g. $I_{g,\text{inlet}}$, possibly depending on time but not on the solution.

In what follows, the dependence of F and g on U and p, and their dependence on (t) will be omitted in the equations. Note that explicit time-dependence, e.g. due to time-dependent source terms or time-dependent boundary conditions, can be accommodated by adding time as an unknown to U and adding the equation $\dot{t} = 1$.

4.2. Derivation of the index and hidden constraints

The index of the DAE system is an important concept that gives the theoretical framework for studying the order conditions and the associated order of accuracy of the time integration methods that will be proposed in section 5. The index and any hidden constraints are revealed by differentiating the DAE system in time:

$$\ddot{U} = \frac{\partial F}{\partial U} \dot{U} + \frac{\partial F}{\partial p} \dot{p}, \tag{74}$$

$$\frac{\partial g}{\partial U} \dot{U} = 0. \tag{75}$$

The differentiated constraint can be rewritten after substituting equation (66):

$$\frac{\partial g}{\partial U} F(U, p) = 0. \tag{76}$$

Evaluating this equation by using equations (67) and (68) gives

$$\frac{\partial g}{\partial U} F(U, p) = \begin{pmatrix} \frac{\partial g}{\partial m} & \frac{\partial g}{\partial I} \end{pmatrix} \begin{pmatrix} F_m \\ F_I \end{pmatrix} = Q F_m = 0, \tag{77}$$

and after substituting equation (69) we obtain:

C1: $\boxed{MI + r = 0,}$ \hfill (78)

with $M = Q D$ and $r = Q b$. For example, with inflow conditions at $s = 0$, and outflow conditions at $s = L$, we have

$$r(t) = \begin{pmatrix} -I_{g,\text{inlet}}(t)/\rho_g - I_{l,\text{inlet}}(t)/\rho_l \\ 0 \\ \vdots \\ 0 \end{pmatrix} = \begin{pmatrix} -V(t) \\ 0 \\ \vdots \\ 0 \end{pmatrix}. \tag{79}$$

Equation (78) is the semi-discrete equivalent of the volumetric flow constraint that was encountered as a Riemann invariant in the characteristic analysis, viz. equation (33).

In contrast to the compressible two-fluid model, a single differentiation does not yield an equation for the pressure, because F_m is not a function of p, i.e. $\frac{\partial g}{\partial U} \frac{\partial F}{\partial p} = 0$. To obtain a pressure equation we need to further differentiate the constraint:

$$\frac{\partial g}{\partial U} \ddot{U} = 0. \tag{80}$$

Note that $\frac{\partial^2 g}{\partial U^2} = 0$, since Q and A in equation (70) are independent of U and t. The constraint (80) is rewritten by substituting (74), leading to

$$\frac{\partial g}{\partial U}\frac{\partial F}{\partial U}F + \frac{\partial g}{\partial U}\frac{\partial F}{\partial p}\dot{p} = \frac{\partial g}{\partial U}\frac{\partial F}{\partial U}F = 0. \tag{81}$$

This equation is the second hidden constraint (C2), the discrete equivalent of the constraint given by equation (36). This constraint can be written in a more convenient form by substituting the expression for F_m, yielding

$$\frac{\partial g}{\partial U}\frac{\partial F}{\partial U}F = -Q\left(D(F_I - Hp) + \dot{b}\right) = -MF_I + MHp - \dot{r} = 0, \tag{82}$$

or

C2: $\boxed{Lp = MF_I + \dot{r}.}$ $\qquad\qquad\qquad\qquad\qquad\qquad\qquad\qquad\qquad\qquad\qquad\qquad\qquad$ (83)

where $L = MH$ is a Laplace operator, being the discrete version of $\frac{\partial}{\partial s}\left(\left(\frac{A_g}{\rho_g} + \frac{A_l}{\rho_l}\right)\frac{\partial p}{\partial s}\right)$. L is symmetric negative definite since the volume fractions are always non-negative. Equation (83) is the Poisson equation for the pressure in incompressible 1D multiphase flow and it corresponds to the pressure constraint C2 derived earlier in equation (38). A further differentiation is required to derive an ODE for the pressure, and to obtain the index of the DAE system:

$$\frac{\partial g}{\partial U}\dddot{U} = 0. \quad (84)$$

Substituting the equation for $\dddot{U}$ (not shown here) into this equation gives an ODE for the pressure, because $\frac{\partial g}{\partial U}\frac{\partial F}{\partial U}\frac{\partial F}{\partial p}$ is non-singular: it is the Laplace operator L. Equivalently, one can take the time derivative of equation (83). Since three differentiations were required to arrive at the ODE for the pressure, the index of the DAE system (66)–(67) is 3. To be precise, the DAE system is in semi-explicit form and has Hessenberg index 3.[2] The existence of solutions for our index 3 problem is guaranteed since F_I is *linear* in p [40].

4.3. Summary

The previous analysis highlights the third novel result of this paper: the semi-discrete pressure equation for incompressible flow can be derived in a structured manner by considering the framework of differential-algebraic equations. The system has index 3 and has the same constraints, C1 and C2 (for the volumetric flow and for the pressure, respectively), that were derived for the continuous equations in section 2.

As graphically shown in the second row of Fig. 1, the index 3 system (66)–(67) can be rewritten in terms of an index 2 system (equations (66) and (78)), or an index 1 system (equations (66) and (83)). This index reduction can be useful in order to apply existing (index 1 or 2) time integration methods. However, care has to be taken that the original constraint C0, (70), is satisfied. In the next section we propose time integration methods based on the index 3 formulation that preserve all three constraints C0, C1 and C2.

5. New time integration methods

5.1. Explicit Runge–Kutta methods

In this section we focus on the third row of Fig. 1: discretization of equations (66)–(67) in time with an explicit Runge–Kutta method. Application of an explicit RK-method is not trivial due to the presence of the constraint, which has to be satisfied at the new stage level, and consequently introduces a degree of implicitness to the system. Related to this issue is the evaluation of the pressure term in the momentum equation. A possible approach is to discretize the pressure equation corresponding to the pressure constraint C2, (83), but this does not directly guarantee compatibility with the Runge–Kutta time integration strategy and the constraint. Instead, we will take the following approach: first, discretize the system of equations with a so-called half-explicit Runge–Kutta method [23], and then perform substitutions on the fully discrete system, such that a fully discrete pressure equation consistent with constraints C0 and C1 will be obtained.

First, we assume that the initial conditions are consistent and that they fulfill the hidden constraints, i.e.

C0: $Q m^0 = A,$ $\qquad\qquad\qquad\qquad\qquad\qquad\qquad\qquad\qquad\qquad\qquad\qquad\qquad\qquad$ (85)

C1: $MI^0 + r(t^0) = 0,$ $\qquad\qquad\qquad\qquad\qquad\qquad\qquad\qquad\qquad\qquad\qquad\qquad\qquad$ (86)

C2: $L^0 p^0 = MF_I^0 + \dot{r}(t^0).$ $\qquad\qquad\qquad\qquad\qquad\qquad\qquad\qquad\qquad\qquad\qquad$ (87)

---

[2] Hessenberg form: ODEs coupled with constraint, with explicit identification of algebraic and differential variables, where the algebraic variables may all be eliminated using the same number of differentiations [5].

The half-explicit Runge–Kutta method for the index 3 system then follows by advancing the differential part of the equations with an explicit procedure, but requiring the constraint to be satisfied at each stage of the Runge–Kutta method:

$$m_i = m^n + \Delta t \sum_{j=1}^{i-1} a_{ij} F_{m,j}, \tag{88}$$

$$I_i = I^n + \Delta t \sum_{j=1}^{i-1} a_{ij}(F_{I,j} - H_j p_j), \tag{89}$$

$$Q m_i = A, \tag{90}$$

followed by an update to the new time level t^{n+1} by combining the stage values, again constrained by the volume constraint:

$$m^{n+1} = m^n + \Delta t \sum_{i=1}^{s} b_i F_{m,i}, \tag{91}$$

$$I^{n+1} = I^n + \Delta t \sum_{i=1}^{s} b_i(F_{I,i} - H_i p_i), \tag{92}$$

$$Q m^{n+1} = A. \tag{93}$$

The subscript i denotes the stage level, and should not be confused with the spatial index used earlier. m_i, I_i and p_i are approximations to $m(t_i)$, $I(t_i)$, $p(t_i)$, where $t_i = t^n + c_i \Delta t$. The coefficients a_{ij}, b_i and c_i form the Butcher tableau that fully defines the Runge–Kutta method.

We stress that equations (88)–(90) *and* (91)–(93) *fully define the time integration method and hence determine its solution. The subsequent 'substitution' steps presented next are simply a reformulation of these equations in order to arrive at a predictor-corrector type algorithm that involves the solution of a Poisson equation.*

The substitution process follows the same route as the semi-discrete case: substitute the mass equations (88) into the constraint (90) to get:

$$\Delta t \sum_{j=1}^{i-1} a_{ij} Q F_{m,j} = A - Q m^n = 0, \tag{94}$$

which becomes, after substituting the expression $F_m = -DI - b$,

$$\sum_{j=1}^{i-1} a_{ij} \left(MI_j + r_j \right) = 0. \tag{95}$$

Since we use an explicit Runge–Kutta method, this reduces to

$$\underline{C1}: \qquad MI_{i-1} + r_{i-1} = 0. \tag{96}$$

In other words, *the volume constraint at stage i can be rewritten in terms of the volumetric flow constraint evaluated at stage $i-1$.* Equation (96) is the fully discrete equivalent of equations (8) and (78).

Subsequently, the expression for I_{i-1} follows from substituting the momentum equation, equation (89), and we obtain:

$$M \left(I^n + \Delta t \sum_{j=1}^{i-2} a_{i-1,j}(F_{I,j} - H_j p_j) \right) + r_{i-1} = 0. \tag{97}$$

Rewriting gives

$$\underline{C2}: \quad a_{i-1,i-2} L_{i-2} p_{i-2} = a_{i-1,i-2} M F_{I,i-2} + \sum_{j=1}^{i-3} a_{i-1,j} \left(M F_{I,j} - L_j p_j \right) + \frac{r_{i-1} - r^n}{\Delta t}. \tag{98}$$

This is the Poisson equation for the pressure p_{i-2}, i.e. the second hidden constraint evaluated at stage $i-2$. In other words, *the volume constraint at stage i leads to the pressure constraint evaluated at stage $i-2$:*

$$Q m_i = A \quad \rightarrow \quad MI_{i-1} + r_{i-1} = 0 \quad \rightarrow \quad L_{i-2} p_{i-2} = \dots \tag{99}$$

For example, in a 3-stage method, p_1 is the pressure that ensures that the velocity field I_2 is divergence free, which in turn makes that the hold-ups m_3 satisfy the volume constraint. This is indicated in Fig. 6. The index 3 nature of the
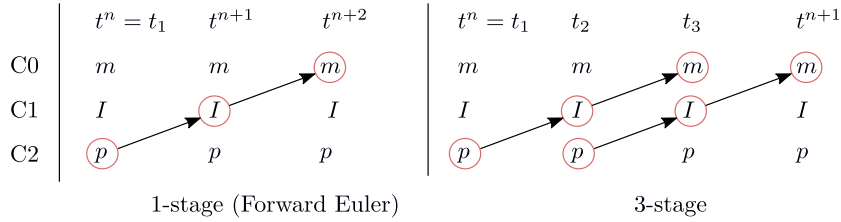
Fig. 6. Example of constraint progression for 1-stage and 3-stage Runge–Kutta method.

system manifests itself in that *two* substitution steps are required to obtain an equation for the pressure, in contrast to the single-phase, index 2 case, where only one substitution is required. This is consistent with the derivation of the pressure equation (83) and the observations in [40].

The pressure equation (98) can be rewritten in a more convenient form by simply changing the indices:

$$a_{i,i-1}L_{i-1}p_{i-1} = a_{i,i-1}MF_{I,i-1} + \sum_{j=1}^{i-2} a_{i,j}\left(MF_{I,j} - L_j p_j\right) + \frac{r_i - r^n}{\Delta t}. \tag{100}$$

With equation (100) we rewrite (88)–(90) into a 'predictor-corrector' algorithm, similar to the fractional-step methods commonly used in incompressible Navier–Stokes algorithms. The first stage is trivial and gives $F_{I,1} = F_I(m_n, I_n, p_n)$ and $F_{m,1} = F_m(I_n)$. The subsequent stages are given by ($i = 2, \ldots, s$)

$$m_i = m^n + \Delta t \sum_{j=1}^{i-1} a_{ij} F_{m,j}, \tag{101}$$

$$I_i^* = I^n + \Delta t \left(\sum_{j=1}^{i-1} a_{ij} F_{I,j} - \sum_{j=1}^{i-2} a_{ij} H_j p_j \right), \tag{102}$$

$$L_{i-1}\phi_{i-1} = MI_i^* + r_i, \tag{103}$$

$$I_i = I_i^* - H_{i-1}\phi_{i-1}. \tag{104}$$

Here we defined ϕ_{i-1} such that $p_{i-1} = \phi_{i-1}/(a_{i,i-1}\Delta t)$. The final update to the new time level $n+1$ is given by

$$m^{n+1} = m^n + \Delta t \sum_{i=1}^{s} b_i F_{m,i}, \tag{105}$$

$$I^{n+1,*} = I^n + \Delta t \left(\sum_{i=1}^{s} b_i F_{I,i} - \sum_{i=1}^{s-1} b_i H_i p_i \right), \tag{106}$$

$$L_s\phi_s = MI^{n+1,*} + r^{n+1}, \tag{107}$$

$$I^{n+1} = I^{n+1,*} - H_s\phi_s. \tag{108}$$

We note the following:

- The solution at the intermediate stages (m_i and I_i) does not depend on the pressure at the start of the time step, p^n.
- The predictor-corrector formulation does not contain a splitting error (see also [43]).
- The Laplace operator $L_i = MH_i$ changes from stage to stage because the gradient operator H_i depends on the solution. An s-stage Runge–Kutta method requires s Poisson solves per time step.
- It is necessary that the subdiagonal of the Butcher tableau, $a_{i+1,i}$, has all entries nonzero.
- There is no start-up problem. The first stage is trivial; the second stage gives $m_2 = m^n + a_{21}\Delta t F_m(I_n)$ which automatically satisfies the volume constraint $Q m_2 = Q m_n = A$, as long as the initial conditions are consistent. Subsequently, ϕ_1 is determined such that I_2 satisfies the volumetric flow constraint $MI_2 + r_2 = 0$, and such that $Q m_3 = Q m^n = A$.

5.2. Accuracy of the Runge–Kutta method

The analysis of the temporal accuracy of Runge–Kutta methods applied to general index 3 DAE systems is not simple – see for example [29,40]. Fortunately, because the volume constraint of the two-fluid model is simple, the fully discrete equations can be rewritten as if they were derived from an index 2 formulation. This is indicated in Fig. 1 by the arrow 'accuracy analysis'. The corresponding index 2 DAE formulation is derived as follows. First write the half-explicit Runge–Kutta method of equations (88), (89) and (96) as

$$U_i = U^n + \Delta t \sum_{j=1}^{i-1} a_{ij} \left(\hat{F}_j - \hat{H}_j p_j \right), \tag{109}$$

$$\hat{M} U_i + r_i = 0, \tag{110}$$

where the extended operators $\hat{(.)}$ are defined as

$$\hat{F}(U) = \begin{bmatrix} F_m(I) \\ F_I(m, I) \end{bmatrix}, \qquad \hat{M} = \begin{bmatrix} 0 & M \end{bmatrix}, \qquad \hat{H}(U) = \begin{bmatrix} 0 \\ H(m) \end{bmatrix}. \tag{111}$$

The gradient operator that acts on the pressure can be written as

$$H(m)p = (Rm) \odot (\hat{G}p) = \mathrm{diag}(Rm)\hat{G}p, \tag{112}$$

where

$$Rm = \begin{pmatrix} R_g & 0 \\ 0 & R_l \end{pmatrix} \begin{pmatrix} m_g \\ m_l \end{pmatrix}, \qquad \hat{G} = \begin{pmatrix} G \\ G \end{pmatrix}. \tag{113}$$

The corresponding semi-discrete system is then recognized as

$$\frac{\mathrm{d}U}{\mathrm{d}t} = F(U, p) \tag{114}$$

$$\hat{g}(U) := \hat{M} U + r = 0. \tag{115}$$

A crucial observation is that this semi-discrete system (and the corresponding half-explicit Runge–Kutta method) has the same form as the single-phase incompressible Navier–Stokes equations, for which the order conditions were shown in [43]. However, there is one important exception in the current multi-phase flow problem: *the pressure gradient term depends on the solution* due to the presence of the hold-up fractions: $H = H(m)$. This dependence leads to additional order conditions for the differential component U for methods of order 3 or higher. These conditions are shown in Table 3 in [43].

For order 3, there is one additional order condition, which reads

$$\sum_{i,j} b_i c_i \omega_{ij} c_{j+1}^2 = \frac{2}{3}, \tag{116}$$

where ω is the inverse of the shifted Butcher tableau $\tilde{a}$:

$$\tilde{a} = \begin{pmatrix} a_{21} & 0 & & \\ \vdots & \ddots & & \\ a_{s1} & & a_{s,s-1} & 0 \\ b_1 & \cdots & b_{s-1} & b_s \end{pmatrix}. \tag{117}$$

The differential associated to order condition (116) is given by condition 10 in [43], which reads

$$F_{pU}(F, (-\hat{g}_U F_p)^{-1} \hat{g}_{UU}(F, F)) = -(RF_m) \odot \hat{G} L^{-1} \ddot{r}, \tag{118}$$

where the right hand side is obtained by inserting system (114)–(115). The dependence of the pressure gradient term on the hold-up fractions manifests itself in the fact that $F_{pU} \neq 0$, which is in contrast to single-phase problems, where generally $F_{pU} = 0$.

Requiring order condition (116) to be satisfied (in addition to the four classic order conditions for a third order Runge–Kutta method [24]), leads to a one-parameter family of methods, with the following Butcher tableau ($c_2 \neq 0$, $c_2 \neq \frac{2}{3}$, $c_2 \neq 1$):

$$
\begin{array}{c|cccc}
0 & 0 \\
c_2 & c_2 \\
1 & 1 + \frac{1-c_2}{c_2(3c_2-2)} & -\frac{1-c_2}{c_2(3c_2-2)} \\
\hline
& \frac{1}{2} - \frac{1}{6c_2} & \frac{1}{6c_2(1-c_2)} & \frac{2-3c_2}{6(1-c_2)}
\end{array}
\tag{119}
$$

<div align="center">RK3</div>

We propose to use the value of $c_2 = \frac{1}{2}$, which is such that the b-coefficients are all positive and such that most order conditions associated to fourth order are also satisfied (leading to a small truncation error).

For order 4, in total six additional order conditions appear [43]. It is shown in [11] that these cannot be satisfied when employing a four-stage method that also should satisfy the classical order conditions. This means that *an explicit four-stage, fourth-order Runge–Kutta method does not exist* for the differential-algebraic equations arising in one-dimensional multiphase flow problems. To achieve fourth order, a five-stage method is needed. An example of a five-stage, fourth-order method that satisfies all additional order conditions is the HEM4 method described in [11].

A crucial remark is in place here. Equation (118) indicates that in case $\ddot{r} = 0$, the additional order condition for third order disappears. It turns out that this is also true for fourth order (see Table 3 in [43]). The case $\ddot{r} = 0$ appears when either

- the boundary conditions are prescribed in weak form; or
- the boundary conditions are prescribed in strong form but they do not depend on time.

In both cases *no additional order conditions are present, and classic Runge–Kutta methods can be used.*

The issue of order reduction and additional order conditions is even more prominent for the accuracy of the pressure. In fact, the pressure p_s obtained from $\phi_s/(b_s \Delta t)$ is generally only a first-order accurate approximation to the pressure $p(t^{n+1})$. However, there is a simple way to make the accuracy of the pressure the same as of the differential variables, namely by solving equation (83), given the solution for m^{n+1} and I^{n+1}:

$$
L^{n+1} p^{n+1} = MF_I^{n+1} + \dot{r}^{n+1}.
\tag{120}
$$

This can be performed as a postprocessing step whenever an accurate pressure is required, since p^{n+1} does not influence the solution in the next time step.

To conclude, the following three Runge–Kutta methods will be considered in our test cases:

$$
\begin{array}{c|c}
c_i & a_{ij} \\
\hline
& b_j
\end{array}
\qquad
\begin{array}{c|cc}
0 & 0 \\
1 & 1 \\
\hline
& \frac{1}{2} & \frac{1}{2}
\end{array}
\qquad
\begin{array}{c|ccc}
0 & 0 \\
\frac{1}{2} & \frac{1}{2} \\
1 & -1 & 2 \\
\hline
& \frac{1}{6} & \frac{2}{3} & \frac{1}{6}
\end{array}
\qquad
\begin{array}{c|cccc}
0 & 0 \\
\frac{1}{2} & \frac{1}{2} \\
\frac{1}{2} & 0 & \frac{1}{2} \\
1 & 0 & 0 & 1 \\
\hline
& \frac{1}{6} & \frac{1}{3} & \frac{1}{3} & \frac{1}{6}
\end{array}
\tag{121}
$$

<div align="center">Tableau   RK2   RK3-proposed   RK4</div>

The second order method is the explicit midpoint method. The third order method is our proposed method: tableau (119) with $c_2 = \frac{1}{2}$. The fourth order method is the classic fourth order method, which for our DAE problem is fourth order accurate only provided that $\ddot{r} = 0$; otherwise it is third order accurate. When necessary, we will compare these methods to the RK3-SSP (strong-stability preserving) method [19] and the five-stage fourth order method HEM4 from [11].

The stability domains of these explicit Runge–Kutta methods can be found in many time integration textbooks, e.g. [12] (note that the treatment of the constraint via the pressure equation is fully implicit and does not affect the stability). For convection-dominated problems (for example in case of the inviscid model), we have shown in previous work that the eigenvalues of the semi-discrete equations lie on the imaginary axis [45]. From a stability point of view, RK3 and RK4 are therefore to be preferred, because the stability domain of these methods contains a part of the imaginary axis.

5.3. Eliminating constraint drift

In the solution of the pressure Poisson equation, (103), numerical errors are generally introduced, for example due to the tolerance setting of an iterative method. This can lead to errors in the constraints C0 and C1, equations (94) and (95), which could potentially accumulate over time. We present an approach to prevent this, based on the ideas outlined in [25]. The most important observation is that, when reformulating the constraint equation to obtain Poisson equation (100), one should *not* substitute $Q m^n = A$ or $M I_j + r_j = 0$, but instead leave these terms inside the equations.

When keeping these terms in the equations, a pressure Poisson equation that is similar to equation (103) follows, but with an additional term that involves the accuracy with which the constraints C0 and C1 have been satisfied. For the intermediate stages ($i = 2, \ldots, s$) the Poisson equation is

$$L_{i-1}\phi_{i-1} = MI_i^* + r_i + \eta_i, \tag{122}$$

$$\eta_i = \left(\sum_{j=1}^{i-1} a_{i+1,j}(MI_j + r_j) - \frac{Q\,m^n - A}{\Delta t} \right) / a_{i+1,i}, \tag{123}$$

and the Poisson equation for the update to the next time step is

$$L_s\phi_s = MI^{n+1,*} + r^{n+1} + \eta^{n+1}, \tag{124}$$

$$\eta^{n+1} = -\frac{Q\,m^{n+1} - A}{\Delta t}/a_{21}. \tag{125}$$

As mentioned, constraint errors can be caused by the accuracy with which the Poisson equation is solved. In principle, the solution of the Poisson equations (122) and (124) is straightforward, since the matrix L is tri-diagonal and symmetric negative definite. This type of equation can be solved efficiently with a direct solver or with a preconditioned conjugate gradient solver. In case pressure boundary conditions are not involved, the pressure is determined up to a constant and consequently the matrix L is singular. In principle, this is not a problem, as long as a constant solution lies in the null space of L. However, a direct solver can have difficulties with such a system and therefore we prefer the conjugate gradient solver, which has been used in the test cases reported here. In section 6.2 we will report on the sensitivity of the constraint accuracy depending on the accuracy of the conjugate gradient solver and show the benefits of using the proposed time integration method including elimination of constraint drift.

5.4. Summary

In this section we have outlined the fourth and main novelty in this paper: a new *constraint-consistent*, high-order accurate time integration method. We have used the *discretize first, substitute next* principle to construct a half-explicit Runge–Kutta method that in a discrete sense possesses the same constraints as the continuous and semi-discrete equations, as derived in sections 2 and 4. A custom-made three-stage, third order method has been derived such that the differential-algebraic nature of the problem does not lead to order reduction for time-dependent boundary conditions.

6. Results

Three test cases are studied in this section to highlight the properties of the proposed Runge–Kutta time integration strategy. The test cases exhibit an increasing level of difficulty in the type of boundary conditions:

- The growth of Kelvin–Helmholtz instabilities on a periodic domain to study the order of accuracy of the time integration methods.
- Sloshing of liquid in a closed tank to study solid wall boundary conditions and to assess constraint accuracy and conservation properties in the presence of shock waves.
- The ramp-up of the gas flow rate in a pipeline to study the order of accuracy for time-dependent boundary conditions, highlighting our proposed RK3 method, which does not suffer from order reduction.

6.1. Kelvin–Helmholtz instability

The Kelvin–Helmholtz instability occurs due to an imbalance between inertial forces (destabilizing) and gravity forces (in terms of density differences, stabilizing). In multiphase flow in pipelines this instability can start from stratified flow and lead to the formation of slug flow. We consider a case similar to the one considered by Liao et al. [33], for conditions where the two-fluid model is *unstable and well-posed*, so we can study the growth of waves that can lead to slug formation. First we find a steady state solution for the parameter values given in Table 1. Choosing $u_l = 1$ m/s and $\alpha_l = 0.9$ yields the gas velocity and the pressure gradient necessary to sustain the steady solution:

$$u_g = 8.0 \text{ m/s}, \qquad \frac{\mathrm{d}p_{\text{body}}}{\mathrm{d}s} = -87.9 \text{ Pa/m}. \tag{126}$$

The velocity difference $u_g - u_l$ is just below the limit given by equation (21), which means that the initial boundary value problem is well-posed.

Secondly, we perturb the steady state by imposing a sinusoidal disturbance with wavenumber $k = 2\pi$ and a very small amplitude. Linear stability analysis [33,45] gives the following angular frequencies ω:

Table 1
Parameter values for the test case with the Kelvin–Helmholtz instability.

Parameter	Value	Unit
ρ_l	1000	kg/m^3
ρ_g	1.1614	kg/m^3
R	0.039	m
p_{outlet}	10^6	N/m^2
g	9.8	m/s^2
μ_g	$1.8 \cdot 10^{-5}$	Pa s
μ_l	$8.9 \cdot 10^{-4}$	Pa s
ϵ	10^{-8}	m
L	1	m

$$\omega_1 \approx 3.22 + 2.00i \text{ s}^{-1}, \tag{127}$$

$$\omega_2 \approx 10.26 - 1.61i \text{ s}^{-1}. \tag{128}$$

The negative imaginary part of ω_2 makes the solution unstable due to exponential growth in time. The linear stability analysis provides an analytical solution involving two waves with these frequencies. We set the perturbation related to ω_1 to zero, implying that a single wave with frequency ω_2 results. The exact solution to the linearized equations is then

$$\boldsymbol{W}(s,t) = \boldsymbol{W}^0 + \text{Re}\left[\boldsymbol{\varepsilon}_2 e^{i(\omega_2 t - ks)}\right], \tag{129}$$

where $\boldsymbol{\varepsilon}_2$ is obtained by choosing the liquid hold-up fraction perturbation as $\hat{\alpha}_l = 10^{-6}$, and then computing the perturbations in the gas and liquid velocity from the dispersion analysis [33]. The initial condition which follows by taking $t = 0$ does not satisfy (86)–(87) exactly, and we therefore perform a projection step to make the initial conditions consistent.

As a consistency check, we have first investigated the accuracy of the entire space-time discretization by comparing the discrete solution to the linearized analytical solution (129) at $t = 1$. Upon refining simultaneously the grid and the time step, second order accuracy is obtained for all solution components, for RK2, the proposed RK3 method, and RK4. This is because the convergence rate is dominated by the second order accuracy of the spatial discretization.

To investigate the temporal accuracy alone, we compute a reference solution $\boldsymbol{W}_{\text{ref}}$ at $t = 1$ s with $N = 40$ volumes and RK4 with a small time step, $\Delta t = 1 \cdot 10^{-4}$ s, so that the temporal error is negligible. The temporal error in the hold-up fraction (scaled by the magnitude of the disturbance) then follows from

$$\epsilon_{A_l, \Delta t} = \frac{\|A_{l,\Delta t} - A_{l,\text{ref}}\|_\infty}{\hat{A}_l}, \tag{130}$$

and similarly for the other solution components. The perturbation is increased to $\hat{\alpha}_l = 10^{-3}$ to avoid errors that are around machine precision. Fig. 7 shows these errors as a function of the timestep. All methods convergence to their design order of accuracy, for both the differential and algebraic components. In this test case there are no boundary conditions (so $r = 0$) and therefore *no* additional order conditions appear, making RK4 an excellent choice.

6.2. Sloshing in a closed cylindrical tank

In this section we present a new and challenging test case for the incompressible two-fluid model: sloshing of liquid and gas in a closed pipe section. In a closed system the mass of both the gas and liquid phase is conserved exactly, and we desire the same property of our numerical algorithm. Furthermore, this test case is well-suited for checking the accuracy of the volume constraint C0 and volumetric flow constraint C1, because any constraint drift or error growth will not be able to 'leave' the domain since there are no outflow boundaries.

The geometry of the problem is shown in Fig. 8. At $t = 0$, the liquid is released and starts flowing towards the left wall, from which it reflects, resulting in a complicated wave pattern in time and space. In an experimental setting this can be accomplished by suddenly tilting the pipe section from its horizontal position, as is done for example in [49] for a liquid–liquid system. The parameter values that we employ are shown in Table 2. The spatial mesh has $N = 80$ finite volumes.

6.2.1. Qualitative analysis

Fig. 9 shows the solution in terms of hold-up fraction, pressure and phase velocities for the first 5 seconds of the simulation. Snapshots of the hold-up fraction and pressure are given in Fig. 10.

A uniform initial condition for all parameters satisfies the volume constraint and volume flow constraint, but not the pressure constraint. The initial condition for the pressure should be determined from equation (87), which results in a pressure that changes linearly along the s direction, due to the effect of gravity (see Fig. 10 right, blue line). Note that the pressure behavior at the boundary is correct without requiring an explicit pressure boundary condition.
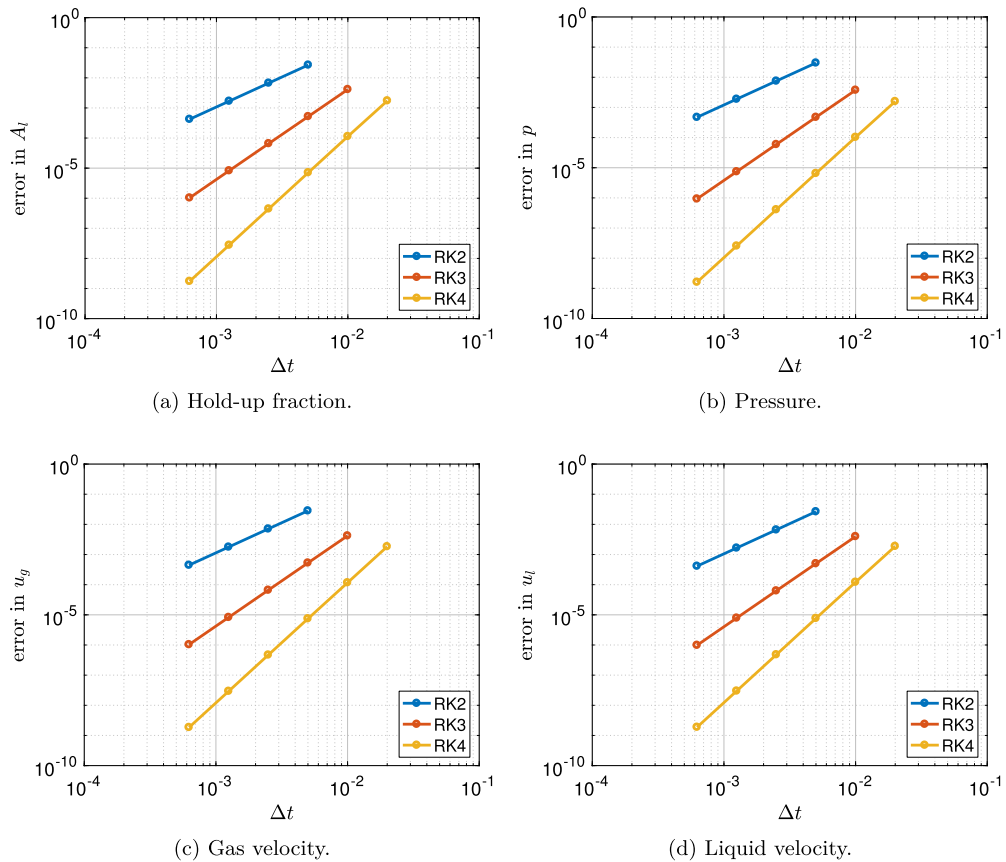
(a) Hold-up fraction.

(b) Pressure.

(c) Gas velocity.

(d) Liquid velocity.

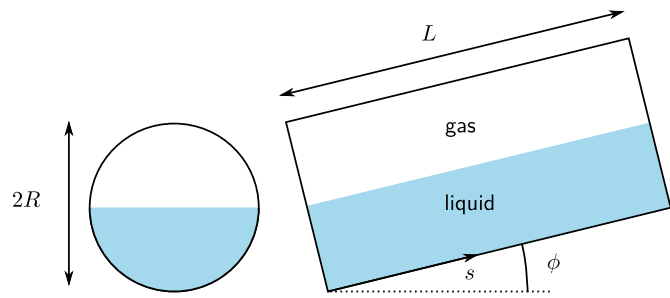**Fig. 7.** Convergence of the temporal error for the incompressible Kelvin–Helmholtz problem.

Fig. 8. Initial condition for sloshing simulation.

Table 2
Parameter values for the closed tank sloshing problem.

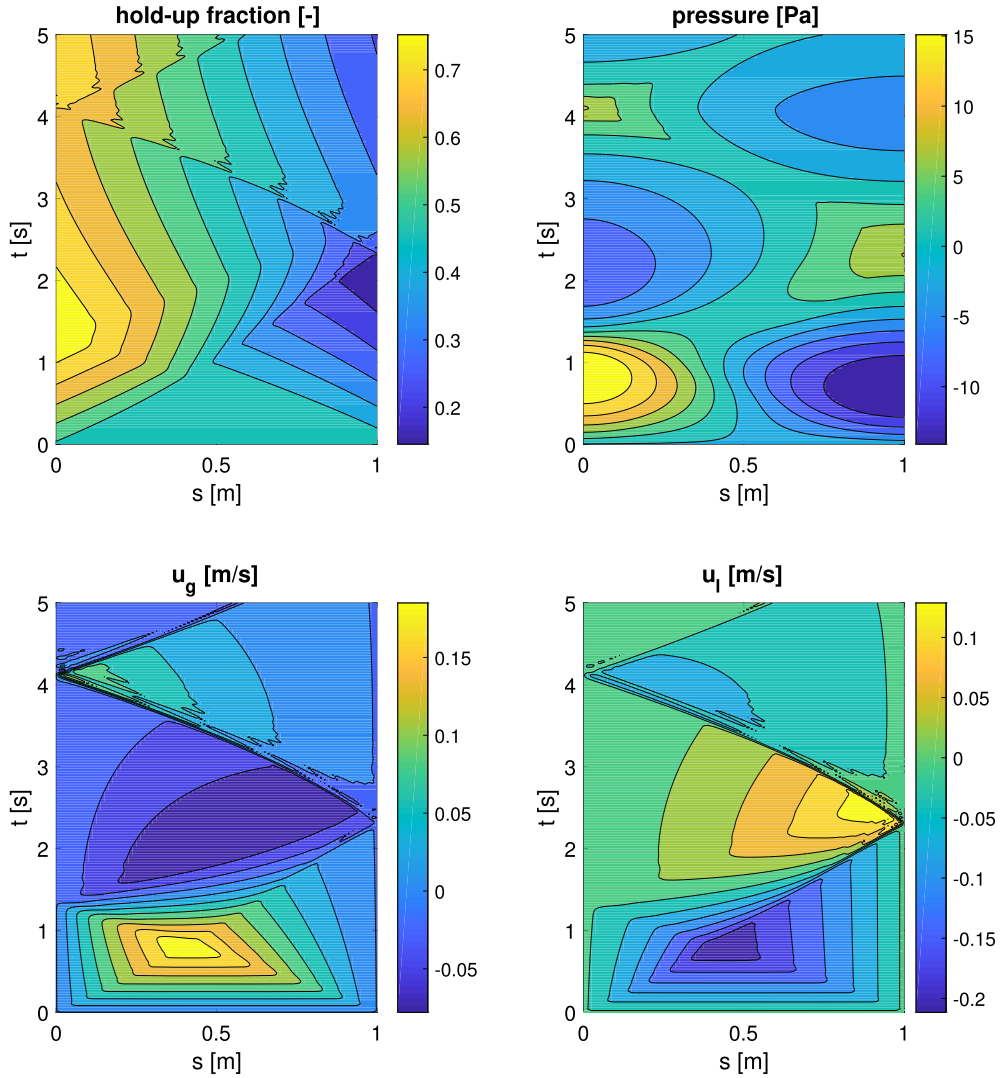| Parameter	Value	Unit
ρ_l	1000	kg/m^3
ρ_g	1.1614	kg/m^3
R	0.05	m
g	9.8	m/s^2
μ_g	$1.5 \cdot 10^{-2}$	Pa s
μ_l	$5.0 \cdot 10^{-2}$	Pa s
ϵ	10^{-8}	m
L	1	m
ϕ	2	deg

Fig. 9. Space-time solution for the sloshing problem with $N = 80$, $\Delta t = 0.02$ and RK4.

The sudden tilting of the pipe section creates two waves, originating from the two boundaries. A compression wave moves to the right, increasing the hold-up fraction and pressure on the left side of the tank. An expansion wave moves to the left, decreasing the pressure and hold-up fraction on the right side of the tank. The expansion wave moves slightly faster than the compression wave and reaches the left side after approximately 1.3 seconds, where it reflects. The compression wave reaches the right side after approximately 2.4 seconds, continues to steepen, and forms a shock wave (this is particularly clear from the plots of the hold-up fraction and the gas velocity). Since central differences are used for the spatial discretization, small wiggles in the solution are present close to the shock front. Other spatial discretization methods, e.g. a Roe-scheme [3], could be employed in order to resolve shocks without oscillations. In principle such methods can be directly used with our time-integration method, as long as the discrete coupling between mass and momentum equations is satisfied, as mentioned in section 3.1. A detail of the solution at $t = 3.5$ seconds is shown in Fig. 10, highlighting the shock wave in the hold-up fraction around $s = 0.5$ m. The pressure, on the other hand, does not exhibit a jump in the solution, but contains a jump in its first derivative, due to the elliptic nature of the Poisson equation.

Without further agitation, the sloshing liquid comes to rest due the action of friction. In Fig. 10 the final steady state (obtained at $t = 50$, when $|u_g|$, $|u_l| < 10^{-8}$) is displayed. In contrast to the initial conditions, the final steady state condition has a uniform pressure value, even though there is more liquid (and therefore hydrostatic head) at the left side of the tank than at the right side. This is because the pressure in the two-fluid model is the *pressure at the interface*. Evaluating the pressure gradient equation, equation (36), for the final quiescent steady state, gives

$$\left(\frac{A_g}{\rho_g} + \frac{A_l}{\rho_l} \right) \frac{\partial p}{\partial s} = -A g_n \frac{\partial h}{\partial s} - A g_s. \tag{131}$$
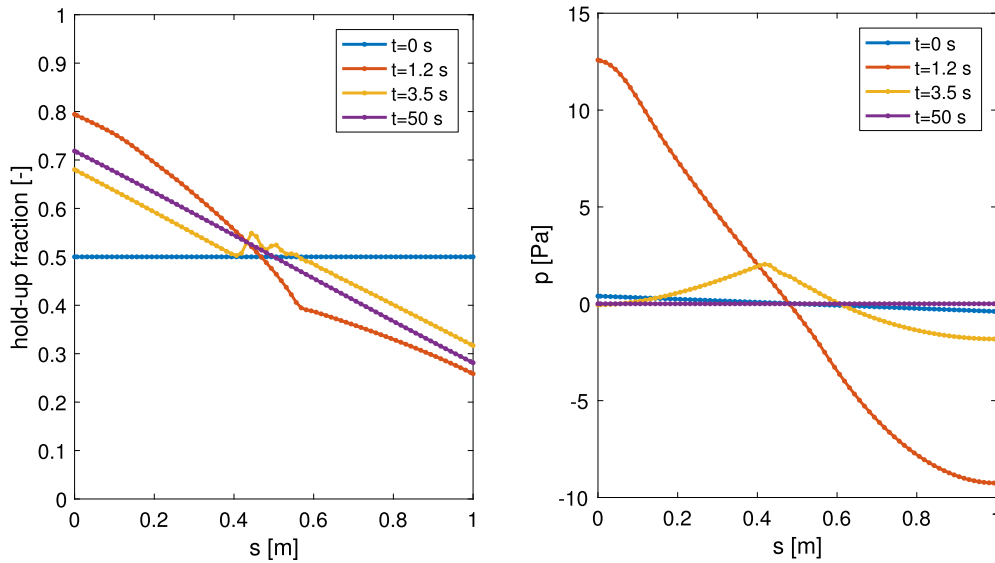
Fig. 10. Details from Fig. 9: initial, intermediate (with shock wave at $t = 3.5$ s) and final solutions for the hold-up fraction (left) and the pressure (right).

Since the steady state attains a level surface, the slope of the liquid is $\frac{\partial h}{\partial s} = -\tan\phi$, and the equation above reduces to

$$\left(\frac{A_g}{\rho_g} + \frac{A_l}{\rho_l}\right)\frac{\partial p}{\partial s} = 0. \tag{132}$$

In physical terms, the hydrostatic head of the liquid is counterbalanced by the level gradient term. Of course, this holds only at the interface; in the lower left corner of the pipe section, for example, the pressure will be higher.

6.2.2. Conservation properties and order of accuracy

Fig. 11a highlights the conservation and constraint properties of our time integration method. When the tolerance of the conjugate gradient solver is sufficiently small, both the volume constraint C0 and the volumetric flow constraint C1 are satisfied until machine precision over the entire course of the simulation. When the threshold of the conjugate gradient solver is increased, the errors in the constraint are larger, but do not drift due to the correction terms proposed in equation (124) (see Fig. 11b). In contrast, when the correction terms as proposed in equation (120) are not taken into account, the volume constraint starts drifting and the drift does not decrease when the solution approaches a steady state (Fig. 11c). Independent of conjugate gradient solver tolerance and correction terms in the pressure equation, the mass of both the gas phase and the liquid phase is conserved until machine precision in all cases (this is a property of the finite volume method).

A temporal accuracy study is performed in the same way as for the Kelvin–Helmholtz test case. We use a reference solution obtained with RK4 and $\Delta t = 10^{-4}$ s to compute the temporal error at $t = 1.2$ s. The resulting convergence of the liquid hold-up fraction, phase velocities, and pressure is shown in Fig. 12. RK2, RK3 and RK4 all converge according to their design order of accuracy. High order accuracy for the pressure is obtained via the solution of equation (120). Besides the high accuracy offered by RK4, we observe here another main advantage: RK4 can be used at larger time steps than RK2 and RK3, due to its larger stability domain. Similar to the first test case, also this test case features $r = 0$, because the boundary conditions for I_g and I_l are independent of time. Therefore, there is no order reduction; RK4 achieves its classical order of accuracy and forms an excellent choice for this test case.

6.3. Perturbed hold-up wave propagation

6.3.1. Test case description

The last test case we perform is the propagation of a hold-up wave, caused by the increase of the gas production at the inlet of a 1 km multiphase pipeline. The test case is inspired by the one proposed by the French Petroleum Institute (IFP) as described by Omgba-Essama [39]. The parameters of the problem are described in Table 3. In contrast to [39], we employ the two-fluid model instead of the homogeneous equilibrium mixture (HEM) model, and therefore require different initial conditions in order to prevent ill-posedness [39] (the HEM model is unconditionally well-posed). The initial conditions are steady state production with inlet mass flows of liquid and gas of $I_l = 1$ kg/s and $I_{g,\text{start}} = 0.02$ kg/s. Furthermore, instead of a linear change in the gas mass flow rate to $I_{g,\text{end}} = 0.04$ kg/s proposed by [39], we employ a sinusoidally varying flow rate, smoothly started from the initial conditions:
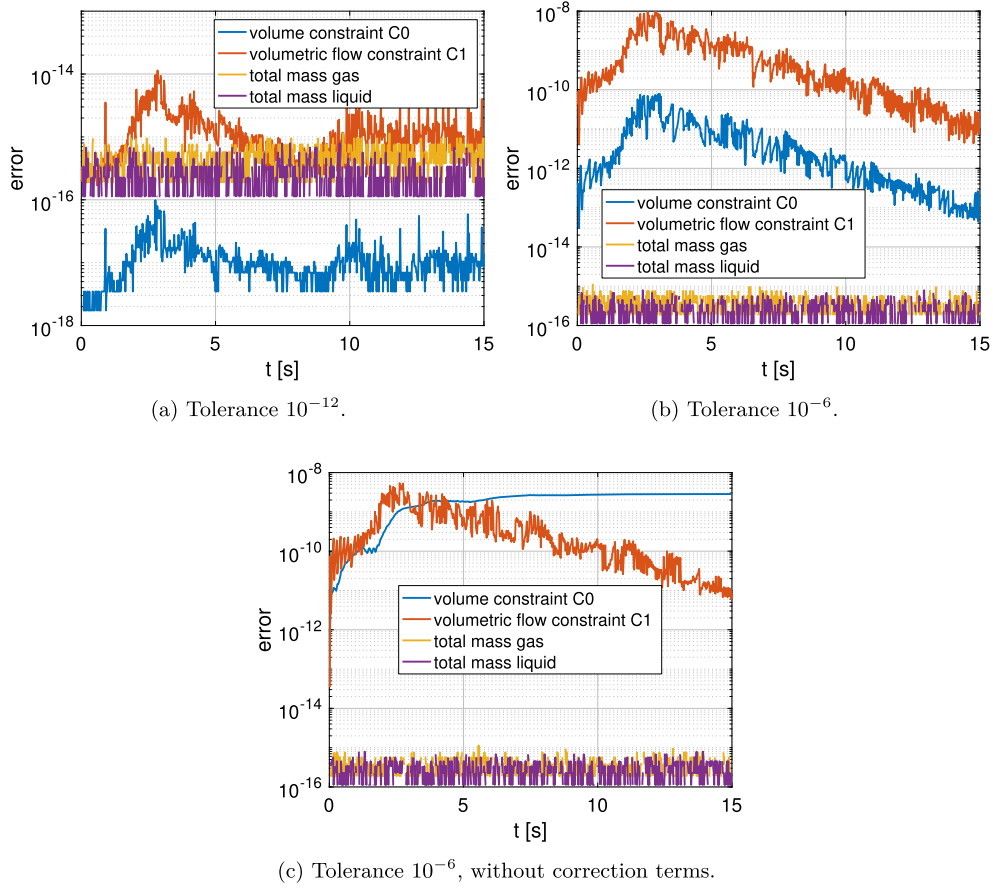
(a) Tolerance 10^{-12}.

(b) Tolerance 10^{-6}.

(c) Tolerance 10^{-6}, without correction terms.

Fig. 11. Error in conservation and constraint properties depending on the tolerance of the conjugate gradient solver, for the sloshing problem with $N = 80$, $\Delta t = 0.02$ and RK4.

Table 3
Parameter values for the IFP problem.

Parameter	Value	Unit
ρ_l	1003	kg/m^3
ρ_g	1.26	kg/m^3
R	0.073	m
p_{outlet}	10^6	N/m^2
g	9.8	m/s^2
μ_g	$1.8 \cdot 10^{-5}$	Pa s
μ_l	$1.516 \cdot 10^{-3}$	Pa s
ϵ	10^{-8}	m
L	1000	m

$$I_g = I_{g,\text{start}} + (I_{g,\text{end}} - I_{g,\text{start}})e^{1-10/t}\left(\frac{1}{2} + \sin(t/5)^2\right)/e^1. \tag{133}$$

The period of oscillation is $5\pi \approx 15.7$ s. This sine-type inflow provides a more severe testcase than a linear ramp-up, because the term $\dot{r}$ in equation (120) contains time-dependent terms.

A qualitative view of the solution behavior in space and time until $t = 150$ s is shown in Figs. 13 and 14. Since the absolute value of the pressure is not important in incompressible calculations, the pressure difference with respect to p_{outlet} is shown. At $t = 0$, all quantities are uniform in space, except the pressure, which decreases as a function of s due to friction losses. Like in the previous test case, the initial condition for the pressure is not prescribed, but is determined by solving equation (87). After a few seconds, the increasing gas mass flow rate leads to a hold-up wave propagating through the pipeline. Two transient effects play a role. First, the gas velocity increases almost instantaneously to adjust for the higher mass flow rate, the liquid velocity increases due to interfacial friction, and the pressure drop increases due to the higher wall friction. This process is repeated given the periodic nature of the inflow. Second, the hold-up fraction starts to slowly adjust following the convection-type equation (2), with a convective velocity determined by the magnitude of the eigenvalues.
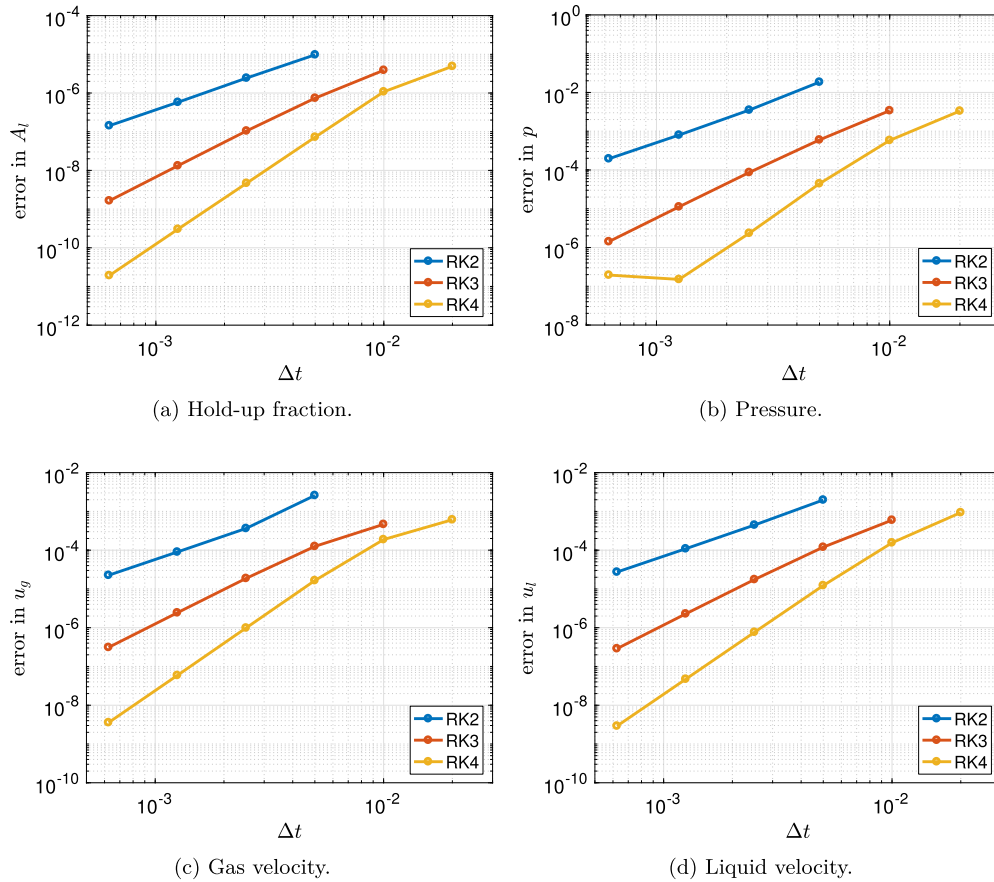
Fig. 12. Convergence of the temporal error for the sloshing problem.

6.3.2. Accuracy study

In order to show the accuracy of the time integration methods, we compare the solution at $t = 100$ s for different time steps and Runge–Kutta methods in Fig. 15. The spatial grid is kept fixed at $N = 40$ volumes, the time step varies from $\Delta t = 20$ s to $\Delta t \approx 10^{-2}$ s, which means that the CFL number at the largest time step (based on the largest eigenvalue) is CFL ≈ 1.5. A reference solution at $N = 40$ with the HEM4 method [11] at very small time step ($\Delta t = 10^{-3}$ s) is used to compute the temporal error, similar to equation (130).

Fig. 15 shows the error in u_l for the case of weak (a) and strong (b) boundary imposition. For weak boundary conditions, all methods converge to the classic (non-DAE) order of convergence, since there are no additional order conditions. The irregular behavior at coarse time steps might be attributed to the fact that the time step is of the same order as the period of the oscillation. Our proposed method, denoted RK3-proposed, converges with almost fourth order for coarse time steps, which can be attributed to the fact that the method satisfies most of the classical fourth order conditions. At small time steps, the third order behavior is recovered. For strong boundary conditions, the effect of order reduction becomes apparent: the RK3-SSP method reduces to second order, whereas our proposed method does not suffer from order reduction. In this test case, the differential associated to the additional order condition (equation (118)) is small, so the order reduction effect is only visible at small time steps. This is also the reason that RK4 does not show order reduction. In Appendix B we show that, for a different test case, also RK4 suffers from order reduction.

7. Conclusions

A new constraint-consistent time integration strategy for the one-dimensional incompressible two-fluid model has been proposed. We have shown that the presence of the volume constraint in the two-fluid model manifests itself on the continuous, semi-discrete, and fully discrete level. On the continuous level, the volume constraint leads to Riemann invariants that correspond to hidden constraints of the model. On the semi-discrete level, the volume constraint leads to an index 3 differential-algebraic equation system, in which the same hidden constraints are present.

On the fully discrete level we have derived a novel time integration strategy, based on high-order 'half-explicit' Runge–Kutta methods, that is consistent with these constraints. Our method is explicit for the mass and momentum equations and
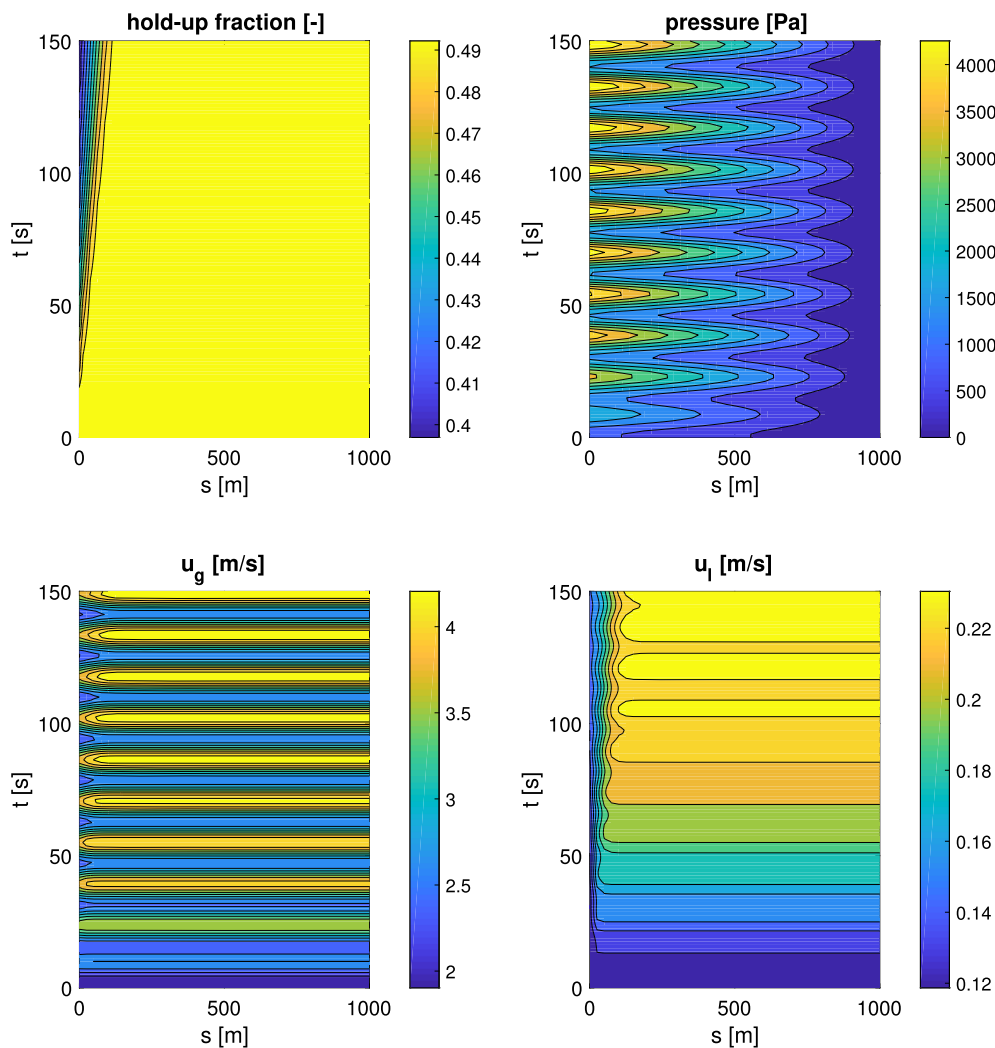
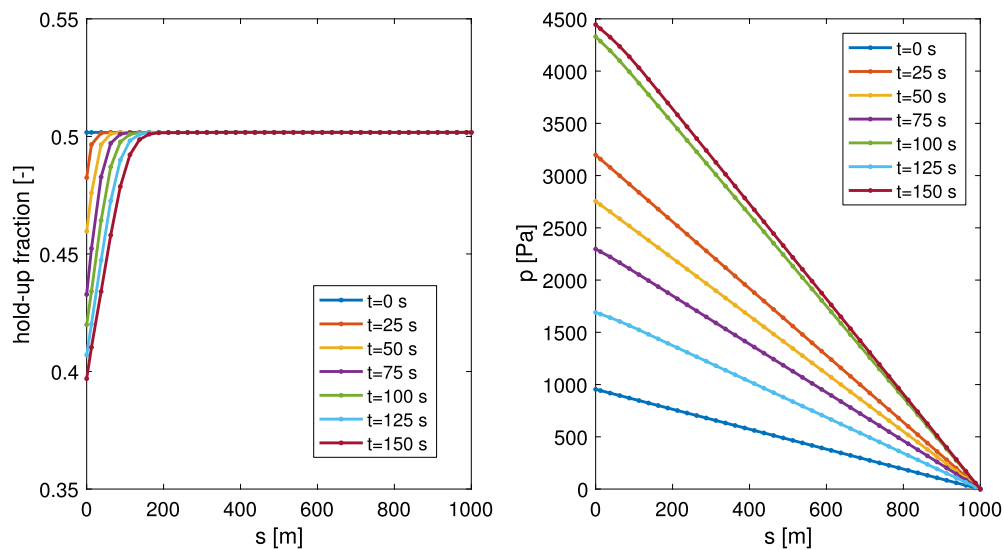**Fig. 13.** Space-time solution for the IFP problem with $N = 40$, $\Delta t = 1.25$ s and the proposed RK3 method.

Fig. 14. Details of Fig. 13 for specific time instances.

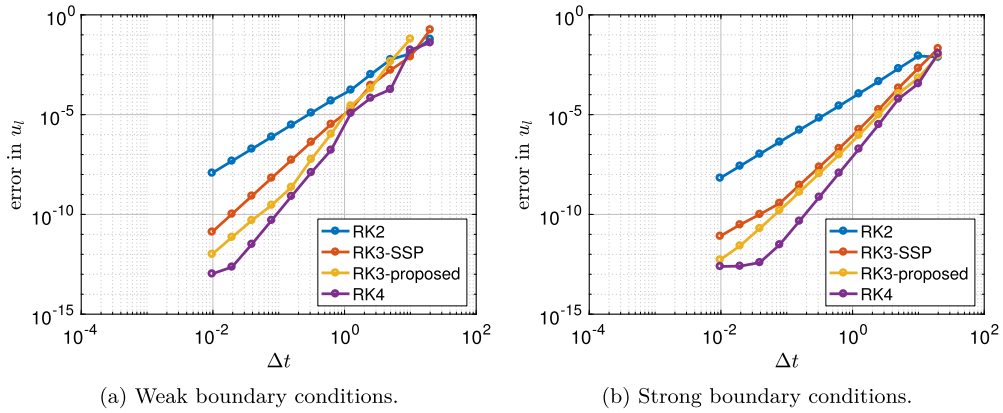(a) Weak boundary conditions.   (b) Strong boundary conditions.

Fig. 15. Convergence of the temporal error in u_l at $t = 100$ s for the IFP problem.

implicit for the pressure. The approach has a fractional-step like character: the pressure at a certain stage (i) of the Runge–Kutta method is such that the mixture velocity field is divergence free at the next stage ($i + 1$), which in turn ensures that the phase masses satisfy the volume constraint at the following stage ($i + 2$). Classic explicit Runge–Kutta methods can be used to achieve high order accuracy, provided that the boundary conditions are time-independent, or prescribed in a weak sense. For the important case of time-dependent boundary conditions prescribed in a strong manner, we have proposed a new three-stage, third order method which does not suffer from order reduction.

Our new time integration method has been demonstrated to perform according to the theoretical analysis for three problems, namely the Kelvin–Helmholtz instability for stratified pipe flow, sloshing in a closed pipe section, and ramp-up of the gas mass flow in a pipeline. It is shown that the classic fourth order Runge–Kutta method performs well for time-independent boundary conditions, but that our proposed third order method is the method of choice for time-dependent boundary conditions.

Several important extensions of the current methodology are possible. First, a larger degree of implicitness can be necessary in certain problems. The current work has focused on half-explicit methods, in which only the pressure is computed implicitly. In case the two-fluid model is extended with terms involving short timescales, for example reaction terms due to thermodynamic phase transitions [34], a higher degree of implicitness might be required. Possible extensions in line with the current work are IMEX (implicit-explicit) methods [4], and partitioned or additive Runge–Kutta methods [30].

Second, different type of constraint systems can be analyzed with our approach, such as the three-fluid model or the drift-flux model. This can shed new light on the wave structure of these models, see e.g. [17], and lead to improved time integration methods and boundary condition treatment. The compressible two-fluid model, see [45], does not possess the same constraint properties as the incompressible model, but the current analysis still provides an important limit that all-speed (incompressible – compressible) solvers should be able to handle.

Lastly, a great potential of our method lies in the extension to multi-dimensional problems, because the DAE analysis and proposed time integration strategy are still valid when the spatial dimension of the problem changes. Example application areas are multiphase flow in reactors [21] and incompressible multiphase flow in reservoirs [7] (in which a saturation constraint similar to the volume constraint is present).

Acknowledgements

Appendix A. Two-fluid model details

A.1. Geometry

The following geometric identities are used to express the wall perimeters, interfacial perimeter, and liquid height in terms of the wetted angle γ_l and pipe diameter $D = 2R$ (see Fig. A.16):

$$P_{gl} = D \sin \gamma_l, \qquad P_l = D \gamma_l, \tag{A.1}$$

$$P_g = D (\pi - \gamma_l), \qquad h = \frac{1}{2} D (1 - \cos \gamma_l). \tag{A.2}$$

We use Biberg's approximation [10] to express α_l in terms of γ_l:
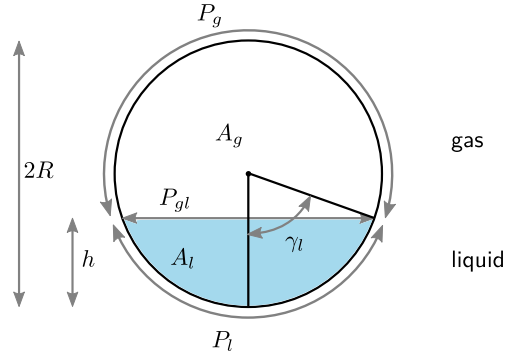
Fig. A.16. Stratified flow layout and definitions.

$$\gamma_l = \pi \alpha_l + \left(\frac{3\pi}{2}\right)^{\frac{1}{3}} \left(\alpha_g - \alpha_l + \alpha_l^{\frac{1}{3}} - \alpha_g^{\frac{1}{3}}\right) - \frac{1}{200}\alpha_l\alpha_g(\alpha_g - \alpha_l)(1 + 4(\alpha_l^2 + \alpha_g^2)). \tag{A.3}$$

A.2. Friction models

The wall (subscript w) and interfacial (subscript gl) shear stress are expressed by the Fanning friction factor definition:

$$\tau = \begin{cases} \dfrac{1}{2} f_\beta \rho_\beta u_\beta |u_\beta| & \text{wall} \\ \dfrac{1}{2} f_{gl} \rho_g (u_\beta - u_\gamma)|u_\beta - u_\gamma| & \text{interfacial} \end{cases} \tag{A.4}$$

The friction factor f_β of phase β with the pipe wall is modeled with the Churchill relation [14]:

$$f_\beta = 2\left(\left(\frac{8}{\text{Re}_\beta}\right)^{12} + (A + B)^{-1.5}\right)^{\frac{1}{12}}, \tag{A.5}$$

$$A = \left(2.457\ln\left(\left(\left(\frac{7}{\text{Re}_\beta}\right)^{0.9} + 0.27\frac{\varepsilon}{D_{h\beta}}\right)^{-1}\right)\right)^{16}, \tag{A.6}$$

$$B = \left(\frac{37530}{\text{Re}_\beta}\right)^{16}. \tag{A.7}$$

Here ε is the hydraulic pipe wall roughness, Re_β is the Reynolds number,

$$\text{Re}_\beta = \frac{\rho_\beta u_\beta D_{h\beta}}{\mu_\beta}, \tag{A.8}$$

and $D_{h\beta}$ is the hydraulic diameter:

$$D_{h\beta} = \begin{cases} \dfrac{4A_l}{P_l} & \text{if } \beta = l \\ \dfrac{4A_g}{P_g + P_{gl}} & \text{if } \beta = g \end{cases} \tag{A.9}$$

The interfacial friction factor f_{gl} is calculated by [33]:

$$f_{gl} = \max(f_g, 0.014). \tag{A.10}$$

Appendix B. Order reduction analyzed with the method of manufactured solutions

In the method of manufactured solutions (MMS) an analytical solution is assumed, substituted into the two-fluid model equations, and the resulting term is used as an additional known source term in the two-fluid model. We design an analytical solution $W^*(s, t)$ which can be exactly represented by the spatial discretization, so that any errors in the numerical
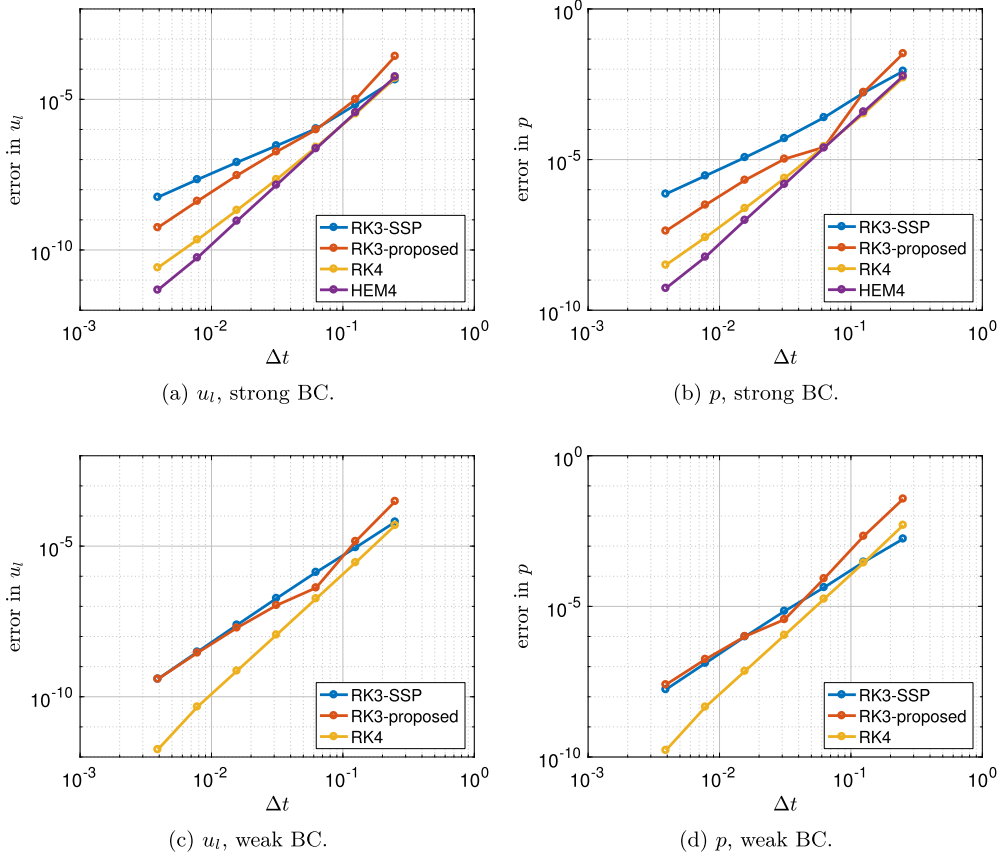
(a) u_l, strong BC.

(b) p, strong BC.

(c) u_l, weak BC.

(d) p, weak BC.

Fig. B.17. Convergence of the temporal error for MMS.

solution are purely due to the time integration method. For this purpose, the phase masses m_g, m_l are chosen to be constant in space, and time-varying according to a prescribed function $f(t)$:

$$m_g^*(s,t) = m_g^*(t) = \rho_g A_g^*(t) = \rho_g \hat{A}_g f(t),$$ (B.1)

$$m_l^*(s,t) = m_l^*(t) = \rho_l A_l^*(t) = \rho_l (A - \hat{A}_g f(t)).$$ (B.2)

The phase momenta are chosen to be linearly varying in space, in such a way that no source term appears in the mass equations:

$$I_g^*(s,t) = m_g^*(t)\hat{u}_g - \dot{m}_g^*(t)s = \rho_g \hat{A}_g \left(\hat{u}_g f(t) - \dot{f}(t)s\right),$$ (B.3)

$$I_l^*(s,t) = m_l^*(t)\hat{u}_l - \dot{m}_l^*(t)s = \rho_l (A_l^*(t)\hat{u}_l + \hat{A}_g \dot{f}(t)s).$$ (B.4)

The phase velocities follow from $u_g^*(s,t) = I_g^*(s,t)/m_g^*(t)$ and similarly for $u_l^*(s,t)$. Note that $u_g^*(s=0,t)$ is constant in time, although $I_g^*(s=0,t)$ is not. For the pressure a linearly varying profile in space is assumed,

$$p^*(s) = c_1 s + c_2.$$ (B.5)

Time dependency could be incorporated in the pressure solution, but is not very important due to the Lagrange-multiplier nature of the pressure.

The additional source term F_{body} required in the momentum equation that forces this analytical solution is then given by

$$\begin{aligned} F_{\text{body},g}(s,t) &= \frac{\partial}{\partial t}\left(I_g^*(s,t)\right) + \frac{\partial}{\partial s}(I_g^*(s,t)u_g^*(s,t)) + \frac{\partial p^*(s)}{\partial s}A_g^*(t) + S_g^*(s,t), \\ &= \rho_g \hat{A}_g(\hat{u}_g \dot{f}(t) - \ddot{f}(t)s) + 2\rho_g \hat{A}_g \left(s\frac{\dot{f}^2(t)}{f(t)} - \hat{u}_g \dot{f}(t)\right) + \hat{A}_g f(t)c_1 + S_g^*(s,t), \end{aligned}$$ (B.6)

where

$$S_g^*(s,t) = S_g(u_g^*(s,t), u_l^*(s,t), A_g^*(t)) \tag{B.7}$$

contains the algebraic source terms (friction and gravity). The level gradient term is zero because the hold-up fractions are uniform in space. The source term for the liquid momentum equation is constructed in a similar fashion.

The function $f(t)$ is chosen to be continuously differentiable with non-vanishing derivatives in order to prevent false perception of high order accuracy. We therefore choose the function

$$f(t) = \frac{1}{60}(\sin(at) + 5)e^{bt}, \quad a = 2, \quad b = 1/20. \tag{B.8}$$

The amplitudes $\hat{A}_g$ and $\hat{u}_g$ are chosen according to the steady state solution.

The parameters of the test case are the same as in section 6.3, except that the pipe length is $L = 10$ m, the diameter is $D = 0.25$ m, laminar friction closure is used, and the initial gas and liquid flow rates are 0.04 and 2 kg/s, respectively. At $s = 0$ unsteady Dirichlet conditions according to (B.8) are prescribed; at $s = L$ outflow conditions are used. We integrate the two-fluid model equations until $t = 20$ s. Fig. B.17 shows the temporal errors for the liquid velocity and the pressure, for both strong and weak boundary conditions. In this test case it is evident that the classic RK schemes RK3-SSP and RK4, not designed for DAEs, suffer from order reduction: RK3-SSP reduces to second order, and RK4 to third order. Our proposed RK3 scheme remains third order. The HEM4 method of [11] is fourth order, but requires five stages, and is therefore less attractive.

References

[1] A. Akselsen, A linear stability analyses of discrete representations of the two-fluid model for stratified two-phase flow, in: ICMF-2016—9th International Conference on Multiphase Flow, May 22–27 2016, Firenze, Italy, 2016.

[2] A.H. Akselsen, Efficient Numerical Methods for Waves in One-Dimensional Two-Phase Pipe Flows, PhD thesis, Norwegian University of Science and Technology, 2016.

[3] A.H. Akselsen, Characteristic methods and Roe's method for the incompressible two-fluid model for stratified pipe flow, Int. J. Multiph. Flow 89 (2017) 81–91.

[4] U. Ascher, S. Ruuth, R. Spiteri, Implicit-explicit Runge–Kutta methods for time-dependent partial differential equations, Appl. Numer. Math. 25 (2–3) (1997) 151–167.

[5] U.M. Ascher, L.R. Petzold, Computer Methods for Ordinary Differential Equations and Differential-Algebraic Equations, Society for Industrial and Applied Mathematics, 1998.

[6] D. Barnea, Y. Taitel, Interfacial and structural stability of separated flow, Int. J. Multiph. Flow 20 (1994) 387–414.

[7] P. Bastian, Numerical Computation of Multiphase Flows in Porous Media, Habilitationsschrift, Universität Kiel, 1999.

[8] K. Bendiksen, D. Malnes, R. Moe, S. Nuland, The dynamic two-fluid model OLGA: theory and application, SPE Prod. Eng. SPE-19451 (1991).

[9] R.A. Berry, J.W. Peterson, H. Zhang, C. Martineau, H. Zhao, L. Zou, D. Andrs, RELAP-7 Theory Manual, Technical report, Idaho National Laboratory, 2014.

[10] D. Biberg, An explicit approximation for the wetted angle in two-phase stratified pipe flow, Can. J. Chem. Eng. 77 (3) (1999) 1221–1224.

[11] V. Brasey, E. Hairer, Half-explicit Runge–Kutta methods for differential-algebraic systems of index 2, SIAM J. Numer. Anal. 30 (2) (1993) 538–552.

[12] J. Butcher, Numerical Methods for Ordinary Differential Equations, John Wiley & Sons, Ltd., 2003.

[13] M.J. Castro, P.G. LeFloch, M.L. Muñoz-Ruiz, C. Parés, Why many theories of shock waves are necessary: convergence error in formally path-consistent schemes, J. Comput. Phys. 227 (17) (2008) 8107–8129.

[14] S.W. Churchill, Friction-factor equation spans all fluid flow regimes, Chem. Eng. 84 (1977) 91–92.

[15] D. Drew, S. Passman, Theory of Multicomponents Fluids, Springer, 1998.

[16] S. Evje, T. Flåtten, CFL-violating numerical schemes for a two-fluid model, J. Sci. Comput. 29 (1) (2006) 83–114.

[17] S. Evje, T. Flåtten, On the wave structure of two-phase flow models, SIAM J. Appl. Math. 67 (2) (2007) 487–511.

[18] G.H. Golub, C.F. van Loan, Matrix Computations, Johns Hopkins University Press, 2012.

[19] S. Gottlieb, C.-W. Shu, E. Tadmor, Strong stability-preserving high-order time discretization methods, SIAM Rev. 43 (1) (2001) 89–112.

[20] P.M. Gresho, R.L. Sani, Incompressible Flow & the Finite Element Method – Advection–Diffusion & Isothermal Laminar Flow, John Wiley & Sons, Ltd, 1998.

[21] A. Guelfi, D. Bestion, M. Boucker, P. Boudier, P. Fillion, M. Grandotto, J.-M. Herard, E. Hervieu, P. Peturaud, NEPTUNE: a new software platform for advanced nuclear thermal hydraulics, Nucl. Sci. Eng. 156 (3) (2007) 281–324.

[22] L.-J. Guo, G.-J. Li, X.-J. Chen, A linear and non-linear analysis on interfacial instability of gas–liquid two-phase flow through a circular pipe, Int. J. Heat Mass Transf. 45 (7) (2002) 1525–1534.

[23] E. Hairer, C. Lubich, M. Roche, The Numerical Solution of Differential-Algebraic Systems by Runge–Kutta Methods, Springer-Verlag, 1989.

[24] E. Hairer, C. Lubich, G. Wanner, Geometric Numerical Integration, Springer-Verlag, 2006.

[25] C. Hirt, F.H. Harlow, A general corrective procedure for the numerical solution of initial-value problems, J. Comput. Phys. 2 (2) (1967) 114–119.

[26] H. Holmås, Numerical Simulation of Waves in Two-Phase Pipe Flow Using 1D Two-Fluid Models, PhD thesis, University of Oslo, 2008.

[27] R. Issa, M. Kempf, Simulation of slug flow in horizontal and nearly horizontal pipes with the two-fluid model, Int. J. Multiph. Flow 29 (1) (2003) 69–95.

[28] R.I. Issa, Solution of the implicitly discretised fluid flow equations by operator-splitting, J. Comput. Phys. 62 (1) (1986) 40–65.

[29] L. Jay, Convergence of Runge–Kutta methods for differential-algebraic systems of index 3, Appl. Numer. Math. 17 (2) (1995) 97–118.

[30] C.A. Kennedy, M.H. Carpenter, Additive Runge–Kutta Schemes for Convection–Diffusion–Reaction Equations, Technical Report NASA/TM-2001-211038, NASA, 2001.

[31] B. Keyfitz, R. Sanders, M. Sever, Lack of hyperbolicity in the two-fluid model for two-phase incompressible flow, Discrete Contin. Dyn. Syst., Ser. B 3 (4) (2003) 541–563.

[32] R. LeVeque, Finite Volume Methods for Hyperbolic Problems, Cambridge University Press, 2002.

[33] J. Liao, R. Mei, J. Klausner, A study on the numerical stability of the two-fluid model near ill-posedness, Int. J. Multiph. Flow 34 (11) (2008) 1067–1087.

[34] R. López, A. Lecuona, J. Nogueira, C. Vereda, Numerical solution of one-dimensional transient, two-phase flows with temporal fully implicit high order schemes: subcooled boiling in pipes, Nucl. Eng. Des. 313 (2017) 319–329.

[35] M. López De Bertodano, W. Fullmer, A. Clausse, V.H. Ransom, Two-Fluid Model Stability, Simulation and Chaos, Springer, 2016.

[36] R. Lyczkowski, D. Gidaspow, C. Solbrig, E. Hughes, Characteristics and stability analyses of transient one-dimensional two-phase flow equations and their finite difference approximations, Nucl. Sci. Eng. 66 (3) (1978) 378–396.

[37] R. Moe, K.H. Bendiksen, Transient simulation of 2D and 3D stratified and intermittent two-phase flows. Part I: theory, Int. J. Numer. Methods Fluids 16 (6) (1993) 461–487.

[38] R. Olsen, Time Dependent Boundary Conditions for Multiphase Flow, PhD thesis, NTNU, 2004.

[39] C. Omgba-Essama, Numerical Modelling of Transient Gas–Liquid Flows (Application to Stratified & Slug Flow Regimes), PhD thesis, Cranfield University, 2004.

[40] A. Ostermann, A class of half-explicit Runge–Kutta methods for differential-algebraic systems of index 3, Appl. Numer. Math. 13 (1993) 165–179.

[41] S.V. Patankar, Numerical Heat Transfer and Fluid Flow, Taylor & Francis, 1980.

[42] D. Picchi, P. Poesio, A unified model to predict flow pattern transitions in horizontal and slightly inclined two-phase gas/shear-thinning fluid pipe flows, Int. J. Multiph. Flow 84 (2016) 279–291.

[43] B. Sanderse, B. Koren, Accuracy analysis of explicit Runge–Kutta methods applied to the incompressible Navier–Stokes equations, J. Comput. Phys. 231 (8) (2012) 3041–3063.

[44] B. Sanderse, S. Misra, S. Dubinkina, R.A.W.M. Henkes, C.W. Oosterlee, Numerical simulation of roll waves in pipelines using the two-fluid model, in: 11th North American Conference on Multiphase Production Technology, 6–8 June, Banff, Canada, BHR Group, 2018, BHR-2018-373.

[45] B. Sanderse, I. Smith, M. Hendrix, Analysis of time integration methods for the compressible two-fluid model for pipe flow simulations, Int. J. Multiph. Flow 95 (2017) 155–174.

[46] B. Sanderse, R. Verstappen, B. Koren, Boundary treatment for fourth-order staggered mesh discretizations of the incompressible Navier–Stokes equations, J. Comput. Phys. 257 (2014) 1472–1505.

[47] H. Stewart, B. Wendroff, Two-phase flow: models and methods, J. Comput. Phys. 56 (1984) 363–409.

[48] K.W. Thompson, Time dependent boundary conditions for hyperbolic systems, J. Comput. Phys. 68 (1) (1987) 1–24.

[49] S.A. Thorpe, Experiments on the instability of stratified shear flows: immiscible fluids, J. Fluid Mech. 39 (1969) 25–48.

[50] I. Toumi, A. Kumbaro, An approximate linearized Riemann solver for a two-fluid model, J. Comput. Phys. 124 (1996) 286–300.

[51] A.E.P. Veldman, "Missing" boundary conditions? Discretize first, substitute next, and combine later, SIAM J. Sci. Stat. Comput. 11 (1) (1990) 82–91.

[52] Z. Wang, J. Gong, C. Wu, Numerical simulation of one-dimensional two-phase flow using a pressure-based algorithm, Numer. Heat Transf., Part A, Appl. 68 (4) (2015) 369–387.

[53] T. Wangensteen, Mixture-Slip Flux Splitting for Numerical Computation of 1-D Two-Phase Flow, PhD thesis, NTNU, 2010.

[54] M. Watson, Wavy stratified flow and the transition to slug flow, in: Multi-Phase Flow – Proceedings of the 4th International Conference, 1989, pp. 495–512.